

**THE FLORIDA STATE UNIVERSITY
COLLEGE OF ARTS AND SCIENCES**

**DEVELOPMENT OF NEW TECHNIQUES FOR ASSIMILATING
SATELLITE ALTIMETRY DATA INTO OCEAN MODELS**

by

PENG YU

**A Dissertation submitted to the
Department of Oceanography
in partial fulfillment of the
requirements for the degree of
Doctor of Philosophy**

**Degree Awarded:
Summer Semester, 2006**

The members of the Committee approve the dissertation of Peng Yu, defended on April 28, 2006.

James J. O'Brien
Professor Directing Dissertation

Xiaolei Zou
Outside Committee Member

William K. Dewar
Committee Member

Allan J. Clarke
Committee Member

Richard Iverson
Committee Member

The Office of Graduate Studies has verified and approved the above named committee members.

Dedicated to my parents,
Guohui Wang, and Michelle Yu.

ACKNOWLEDGEMENTS

I would like to thank Dr. James J. O'Brien, my major professor, for his continuous support and instruction. My sincere appreciation goes to Dr. Steven Morey for all his efforts throughout my research. I would like to acknowledge my committee members Dr. Xiaolei Zou, Dr. Allan Clarke, Dr. William Dewar, and Dr. Richard Iverson for spending time helping me. I want to thank Dr. Jorge Zavala-Hidalgo for helping me with part of this project. I also would like to thank Dr. Paul Martin and Dr. Alan Wallcraft at the Naval Research Laboratory for the NCOM development and assistance with the model.

Funding for this research was provided by the Office of Naval Research, Secretary of the Navy grant awarded to Dr. James J. O'Brien, NASA, and NSF.

TABLE OF CONTENTS

List of Figures	vi
Abstract	viii
1. INTRODUCTION	1
1.1 Review of Data Assimilation Methods	1
1.2 Variational Data Assimilation	5
1.3 Plan of Dissertation	7
2. METHODOLOGY AND DATA	9
2.1 The Reduced Space Variational Data Assimilation Method	9
2.2 Vertical Normal Mode Decomposition	12
2.3 Numerical Optimization	15
2.4 TOPEX/Poseidon and Jason-1 Altimeter Data	17
2.5 Mapping Satellite Altimeter Data	18
2.6 The Ocean Model	22
3. EXPERIMENTS AND RESULTS	27
3.1 Idealized Experiment One	27
3.2 Idealized Experiment Two	36
3.3 Experiment Three: Application to Real Data	45
4. DISCUSSION	53
5. SUMMARY	57
APPENDIX A	60
APPENDIX B	68
REFERENCES	73
BIOGRAPHICAL SKETCH	77

LIST OF FIGURES

- 2.1. The flowchart of the reduced-space variational data assimilation technique. The models are run for the assimilation window $t=[0, T]$, and the forward model solution at time $t=T$ can be used to initialize a forecast 11
- 2.2. The density profile to which vertical normal mode decomposition is applied. Right: Eigenvectors R associated with the first three baroclinic modes. Blue solid line: mode one; Red dashed line: mode two; Black dotted line: mode three 13
- 2.3. The TOPEX/Poseidon and Jason-1 ground tracks in the Gulf of Mexico. Red lines: T/P ground tracks; blue lines: Jason-1 ground tracks..... 19
- 2.4. The interpolation of a sine wave propagating to the right. Positions shown are $t=0$ (blue) and $t=32$ (hatched). Interpolation results (red) at positions at $t=7, 14, 21, 28$ are shown. The left panels show results based on linear interpolation, and the right panel panels show results based on the new mapping method 25
- 2.5. A synthetic eddy propagating westward (left) and the field produced by application of the CEOF mapping method (right) applied to simulated satellite “observations” at yellow dots..... 26
- 3.1. The model domain (98.15°W – 80.60°W , 15.55°N – 31.50°N) and topography for the NCOM simulations used in this work 28
- 3.2. The SSH fields from the model control run in idealized experiment one (used as “observations”) at model day 0 (top) and model day 9 (bottom)..... 30
- 3.3. The normalized cost function (top) and the normalized gradient norm (bottom) with respect to the iteration number in experiment one 32
- 3.4. SSH synoptic maps (at model day 9) of the initial guess (top) and iteration 10 (bottom)..... 33
- 3.5. The root mean square error (RMSE) of SSH of the initial guess (top) and iteration 10 (bottom) computed from the control run SSH fields..... 34
- 3.6. The 18°C isotherm depth (at model day 9) of the “truth”, or control run (top), the first guess (lower left) and iteration 10 (lower right) 35

3.7. (a) Top left: Control run (“truth”) SSH field from experiment two. Top right: SSH field constructed by applying the CEOF mapping technique to values sampled along locations corresponding to T/P and Jason-1 observation locations (black dots) every ten days. Bottom: Difference between the two SSH fields. All fields are from model day 0.....	37
3.7. (b) Same as Figure 3.7(a) except that the results at model day 5 are shown.....	38
3.7. (c) Same as Figure 3.7(a) except that the results at model day 9 are shown.....	39
3.8. The normalized cost function (top) and the normalized gradient norm (bottom) with respect to iteration number for experiment two	40
3.9. (a) The SSH and surface velocity synoptic maps of the initial guess at model day 0 (top) and model day 9 (bottom).....	41
3.9. (b) The SSH and surface velocity field synoptic maps at model day 0 (top) and model day 9 (bottom) of iteration 13.....	42
3.10. The RMSE of SSH of the initial guess (top) and iteration 13 (bottom) computed from the control run SSH fields.....	43
3.11. The RMSE of SSH following a 10-day forecast from the first guess (top) and from iteration 13 (bottom).....	44
3.12. Synoptic maps of the gridded SSH fields produced using CEOF mapping method applied to T/P and Jason-1 data shown at model day 0 (January 9, 2004) and model day 9 (January 18, 2004).....	47
3.13. The normalized cost function (top) and the normalized gradient norm (bottom) with respect to the iteration number for experiment three.....	48
3.14. (a) Synoptic maps of SSH and surface velocity for the initial guess at model day 0 (top) and model day 9 (bottom).....	49
3.14. (b) Synoptic maps of SSH and surface velocity during iteration 14 at model day 0 (top) and model day 9 (bottom).....	50
3.15. The RMSE of SSH of the initial guess (top) and iteration 14 (bottom) computed with respect to the gridded observation fields.....	51
3.16. SSH RMSE between the model and the along-track satellite altimeter data plotted against iteration number	52

ABSTRACT

State of the art fully three-dimensional ocean models are very computationally expensive and their adjoints are even more resource intensive. However, many features of interest are approximated by the first baroclinic mode over much of the ocean, especially in the lower and mid latitude regions. Based on this dynamical feature, a new type of data assimilation scheme to assimilate sea surface height (SSH) data, a reduced-space adjoint technique, is developed and implemented with a three-dimensional model using vertical normal mode decomposition. The technique is tested with the Navy Coastal Ocean Model (NCOM) configured to simulate the Gulf of Mexico.

The assimilation procedure works by minimizing the cost function, which generalizes the misfit between the observations and their counterpart model variables. The “forward” model is integrated for the period during which the data are assimilated. Vertical normal mode decomposition retrieves the first baroclinic mode, and the data misfit between the model outputs and observations is calculated. Adjoint equations based on a one-active-layer reduced gravity model, which approximates the first baroclinic mode, are integrated backward in time to get the gradient of the cost function with respect to the control variables (velocity and SSH of the first baroclinic mode). The gradient is input to an optimization algorithm (the limited memory Broyden-Fletcher-Goldfarb-Shanno (BFGS) method is used for the cases presented here) to determine the new first baroclinic mode velocity and SSH fields, which are used to update the forward model variables at the initial time.

Two main issues in the area of ocean data assimilation are addressed: 1. How can

information provided only at the sea surface be transferred dynamically into deep layers?

2. How can information provided only locally, in limited oceanic regions, be horizontally transferred to ocean areas far away from the data-dense regions, but dynamically connected to it?

The first problem is solved by the use of vertical normal mode decomposition, through which the vertical dependence of model variables is obtained. Analyses show that the first baroclinic mode SSH represents the full SSH field very closely in the model test domain, with a correlation of 93% in one of the experiments. One common way to solve the second issue is to lengthen the assimilation window in order to allow the dynamic model to propagate information to the data-sparse regions. However, this dramatically increases the computational cost, since many oceanic features move very slowly. An alternative solution to this is developed using a mapping method based on complex empirical orthogonal functions (EOF), which utilizes data from a much longer period than the assimilation cycle and deals with the information in space and time simultaneously. This method is applied to map satellite altimeter data from the ground track observation locations and times onto a regular spatial and temporal grid.

Three different experiments are designed for testing the assimilation technique: two experiments assimilate SSH data produced from a model run to evaluate the method, and in the last experiment the technique is applied to TOPEX/Poseidon and Jason-1 altimeter data. The assimilation procedure converges in all experiments and reduces the error in the model fields. Since the adjoint, or “backward”, model is two-dimensional, the method is much more computationally efficient than if it were to use a fully three-dimensional backward model.

1. INTRODUCTION

Measurements of the ocean environment are difficult and expensive, especially within the deep ocean. As a result, oceanic data are usually sparser than their atmospheric counterparts and are non-uniformly sampled in time and space. The launch of many ocean observing satellites over recent decades has yielded a vast amount of data for the ocean's surface. In order to deepen and broaden our understanding of ocean circulation, it is very important to optimize the use of these expanded but still insufficient valuable datasets. This requires the blending of present observations with the theoretical knowledge from past observations, incorporated into numerical models.

Numerical models can be used to assimilate oceanographic data, creating a dynamically consistent, complete and accurate depiction of the three-dimensional time-dependent ocean state. One key problem for oceanographic applications is how to determine variables not directly observed at many locations, such as the velocity, from available observed variables, such as sea surface height (SSH). The answer lies in the dynamical coupling between variables, which is a central role that dynamics plays in estimating the state of the ocean from incomplete data.

1.1 Review of Data Assimilation Methods

Data assimilation is a powerful tool for extracting the maximum amount of information from observations and has been extensively used in numerical atmospheric

and oceanic modeling. In order to assimilate observations into numerical ocean models, there exist a variety of different methods, most of which were originally developed in meteorology. An extensive review of these methods can be found in Ghil and Malanotte-Rizzoli (1991) and Le Dimet and Navon (1988). Data assimilation methods can be classified as function fitting methods, statistical interpolation methods, nudging data assimilation, variational (adjoint) methods and Kalman Filtering techniques.

One of the early and simple data assimilation methods is function fitting, in which the analysis function is expanded in a finite series of ordered mathematical basis functions with unknown expansion coefficients. The coefficients are determined by either an exact fit to observations (analyzed values are required to be equal to observed values at observation locations) or through a least-square fit between the analysis and observations. Once the coefficients are determined, the analyzed variables can be evaluated at any location within the analysis domain. The first attempt of using function fitting for objective analysis dated back to 1949 (Panofsky). In his study, a cubic polynomial regional fitting was applied with arbitrarily specified constant weightings. Gilchrist and Cressman (1954) conducted another study of local quadratic fitting.

This method is linear in the sense that an analysis could always be expressed as a linear combination of observations:

$$x(i) = \sum_{k=1}^K W_{ik} y_k^{obs} , \quad (1.1)$$

where the index i represents the analysis grid, the index k represents observation locations, and the *a posteriori* determined weights W_{ik} are independent of observations. The way the observational information is spread to different regions and/or different variables is solely determined by W_{ik} , which usually decreases with distance from the observation

(Bergthorsson and Doos, 1955). Neither the knowledge of the statistical properties of the data nor a numerical model is used (Thiebaut and Pedder, 1987; Daley, 1991). It is worth mentioning that some dynamical constraints, such as a geostrophic balance constraint, could be incorporated into the analysis and a weak or strong constraint can be imposed through a least-squares fit or a Lagrange multiplier.

The optimal interpolation (OI) or statistical interpolation approach combines the model background field and the observation field to obtain the optimal estimate field, which minimizes the analysis error covariance. This method takes the form of an analysis equation as

$$x^a(\vec{r}_i) = x^b(\vec{r}_i) + \sum_{k=1}^{K_i} \omega_{ik} [x^{obs}(\vec{r}_k) - x^b(\vec{r}_k)] \quad (1.2)$$

where x^a is the analysis field, x^b is the background field, x^{obs} is the observation field, \vec{r}_i is the analysis or background location, \vec{r}_k is the observation location, and ω_{ik} is the weighting function. There are two major differences between function fitting and OI. A background field is introduced into the analysis procedure and the *a posteriori* weights are determined statistically based on background and observation error covariance instead of depending purely on the interpolation function as in function fitting. The knowledge of spatial error covariance for both the model field and the observations is required (Lorenz, 1981, 1988), and a good estimate of these is one of the key factors of the quality of the interpolated field.

The Kalman filter (Kalman, 1960, 1961) represents a sequential assimilation procedure, based on the statistical concept of OI. At each observation time, the Kalman filter conducts an optimal interpolation of the model forecast field and the observations to obtain a new state vector with reduced error covariance. This state is subsequently used

as the initial state for the model to compute a forecast for the next observation time. By repeating this assimilation cycle and keeping track of the error covariance of the model state in a sequential manner, the model absorbs the information of the sequence of observations step by step (Cohn, 1982; Ghil *et al.*, 1981). The Kalman filter is very similar to OI, but with one major difference: the forecast or background error covariance is advanced using the model itself, rather than estimating it as a constant covariance matrix (Kalnay, 2002). The biggest problem with this method is its computational cost, especially for the nonlinear case. A simplification is the extended Kalman filter, which is derived from the basic Kalman filter to nonlinear dynamics by linearization at each time step. Another simplification of Kalman filtering is ensemble Kalman filtering, using Monte Carlo sampling in the propagation step. In this approach, an ensemble of K data assimilation cycles is carried out simultaneously (Houtekamer *et al.*, 1998, 2001, Anderson, 2001).

The nudging data assimilation (NDA) method (Anthes, 1974), which is called optimal nudging data assimilation in the work of Zou *et al.* (1992), relaxes the model state towards the observations during the assimilation period by adding a non-physical diffusive term to the model equations. The goal is to find the best initial state for numerical weather prediction (NWP) and optimal nudging coefficients which best assimilate the given observations.

The variational data assimilation method tries to find an optimal initial condition and/or model parameters which minimize the differences between the observations and the model solution based on optimal control theory. It requires an adjoint model to obtain the gradient of the cost function with respect to the control variables.

1.2 Variational Data Assimilation

The first application of variational methods was by Sasaki (1955, 1958) in meteorology. Sasaki (1969, 1970a, 1970b, 1970c) has made further efforts in developing variational methods and generalizing the application of variational methods in meteorology to include time variations and dynamical equations in order to filter high-frequency noise and to obtain dynamically acceptable initial values in data void areas. The four-dimensional (4-D) Variational approach was first introduced as early as the 1980's (Le Dimet and Talagrand, 1986; Derber, 1987; Talagrand and Courtier, 1987; Courtier and Talagrand, 1987) and has been the subject of further study (Courtier and Talagrand, 1990; Yu and O'Brien, 1991; Zou *et al.*, 1995; Zou *et al.*, 1997). Its fundamental concept is to find an optimal state by minimizing the distance between a model solution and observations (cost function) while at the same time satisfying the dynamical constraints.

The variational data assimilation technique is a novel, versatile methodology for estimating oceanic variables. It requires knowledge of ocean science, computational science, statistics, optimal control theory, and observations. Ocean science provides the fundamental concepts, or the dynamical principles, which govern the system under observation. With knowledge of computational science, the governing equations are translated into numerical models, which can be solved by computers. Knowledge of statistics and observations is also crucial for many aspects, such as the definition of the cost function, the analysis of errors in the whole system. Optimal control theory has significantly advanced data assimilation research. It offers a deterministic approach of the estimation problem posed by the data assimilation method.

Oceanic models are constructed based on physical laws that govern the temporal evolution of the oceanic flows of interest. A numerical model predicts values of future ocean states from specified values of input parameters, which include initial conditions,

boundary conditions, and many other parameters. Let us consider a model

$$F(\mathbf{x}) = 0 \quad (1.3)$$

where \mathbf{x} is a vector of ocean state variables. Suppose some observations \mathbf{y}^{obs} of the variable \mathbf{x} exist over the model domain. The variational data assimilation is defined as a search, amongst all the possible solutions of this model, for the solution closest to the observations. This distance between the model solution and the observations becomes the cost function, which takes the form of

$$J(\mathbf{x}) = \int_{\Sigma} \|g(\mathbf{x}) - \mathbf{y}^{obs}\| ds \quad (1.4)$$

where $g(\mathbf{x})$ is the estimate of model state variables over the observation locations and $\| \cdot \|$ is a norm.

This is an optimization problem, which requires the minimization of the cost function (1.4) under constraint of the model governing equations (1.3). Applying the Lagrange multiplier, the above constrained optimization problem turns into an unconstrained minimization problem of

$$L(\mathbf{x}, \boldsymbol{\lambda}) = J(\mathbf{x}) + \langle \boldsymbol{\lambda}, F(\mathbf{x}) \rangle \quad (1.5)$$

where $\langle \mathbf{a}, \mathbf{b} \rangle$ is an inner product of \mathbf{a} and \mathbf{b} , and $\boldsymbol{\lambda}$ is the Lagrange multiplier.

It can be easily shown that the solution of the constrained optimization problem is equivalent to finding the stationary point, the optimal solution, of (1.5) with respect to variables \mathbf{x} and $\boldsymbol{\lambda}$.

Differentiating L with respect to λ recovers the model governing equation (1.3) and differentiating L with respect to \mathbf{x} leads to

$$0 = \frac{\partial L}{\partial \mathbf{x}} = \frac{\partial J}{\partial \mathbf{x}} + \left\langle \lambda, \frac{\partial F}{\partial \mathbf{x}} \right\rangle. \quad (1.6)$$

(1.6) is called the adjoint model. It is also called the “backward” model, since it is integrated backward in time (see details in Le Dimet and Talagrand, 1986). The solution of (1.6) at the initial time is the gradient of the cost function, L , with respect to the model control variables.

1.3 Plan of Dissertation

The main goal of this research is to develop a new data assimilation technique based on the variational method, and to apply it to a realistic numerical ocean model for testing and demonstration. In this new method, the adjoint model is simplified by approximating the ocean model variable fields by their first baroclinic mode counterparts. Vertical normal mode decomposition is applied in each assimilation cycle to retrieve the first baroclinic mode information from the forward model and to convert the fully three-dimensional problem into a two-dimensional one. The projection of the two-dimensional field onto three dimensions with the first baroclinic mode vertical profile connects the mode one variables to the three-dimensional full model variables and allows the information from the ocean surface to transfer to deep layers. A new method is developed to map SSH observations along satellite altimeter ground tracks to a regular grid. Applying this method over a long time period considers observations that are outside the actual assimilation window, thus reducing the length of the window.

Three experiments are conducted for testing purpose. Experiment one begins with a perturbed initial condition, and assumes a full model grid SSH “observations”. Experiment two simulates a more realistic scenario by sampling the SSH observations in a similar manner as the satellite altimeters (along satellite ground tracks). The mapping method is applied before the assimilation. The last experiment is an application of the technique using observations from TOPEX/Poseidon (T/P) and Jason-1 satellite altimeters.

The assimilation procedure is designed to adjust the model initial conditions. The improved initial conditions will result in the model better simulating the ocean state within the assimilation window, yielding an improved analysis with which an ocean forecast can be initialized. Several assumptions are made in the reduced space variational data assimilation technique, which lead to a more efficient way of assimilating the observations into the model system at a cost of a non-perfect convergence of the cost function.

2. METHODOLOGY AND DATA

A new method of implementing the variational data assimilation technique is developed and explained in this chapter. The method consists of several components, connected in a modular fashion that can be applied to a number of three-dimensional ocean models. For this research, the Navy Coastal Ocean Model (NCOM) is chosen as the “forward” model for testing the method. The adjoint, or backward model for the variational method, is developed from a simplified model, a one-active-layer reduced gravity model. The forward and backward models are connected through vertical normal mode decomposition and reconstruction. These components form the data assimilation system when iterated within an optimization algorithm (see the flowchart in Figure 2.1). This new technique is designed to efficiently assimilate satellite altimeter data, which can be mapped to a uniform grid using a new method developed as part of this work, into the three-dimensional ocean model. The data and each of the assimilation system components are described below.

2.1 The Reduced Space Variational Data Assimilation Method

Oceanic state variables can be dynamically decomposed into different vertical normal modes, where each individual mode or the combination of several modes accounts for different phenomena. Previous work (Dewar and Morris, 2000; Dewar and Huang, 2001; Shu and Clarke, 2002) shows that many oceanic features of interest can be approximated by the top several baroclinic modes. It has been suggested (Liu, 1999)

that the SSH variability is mainly associated with the first baroclinic mode. For example, Siegel *et al.* (1999) showed that in the subtropical North Atlantic, the first baroclinic mode explained 88.5% of the SSH anomaly variance using hydrographic and satellite altimeter data. A similar analysis conducted within the Gulf of Mexico model domain used for this present research reveals that the first baroclinic mode accounts for around 80% of the total variance. Since the satellite altimeter SSH data are assimilated in this application, it is reasonable to reduce the dimensions of the assimilation problem by using a reduced gravity adjoint model, which closely approximates the first baroclinic mode. This assimilation method is different from the conventional adjoint technique, in which the forward and backward models are based on the same dynamics.

The variational assimilation procedure works by minimizing a cost function, the data misfit between the SSH observations and their counterpart model variables. For this research, the assimilation method is applied to a three-dimensional time-dependent forward ocean model that is integrated within the assimilation window. Instead of constructing and running an adjoint model based on the fully three-dimensional forward model as in the conventional adjoint data assimilation technique, an adjoint model based on a one-active-layer reduced gravity model, which approximates the first baroclinic mode, is developed. The different forward and backward models are dynamically connected through vertical normal mode decomposition, which retrieves the first baroclinic mode information from the outputs of the forward model and inputs it into the backward model. After the integration (backward in time) of the approximate adjoint model, the gradient of the cost function with respect to the control variables (velocity and SSH associated with the first baroclinic mode) is obtained as an input to an optimization routine (here, the limited memory BFGS (L-BFGS) method is used). The optimization algorithm updates the first baroclinic mode velocity and SSH fields, which are then used to update the full forward model variables by reconstructing the model fields from the vertical modes (with the newly updated first mode) as described in section 2.2. This procedure repeats until a prescribed convergence criterion is met.

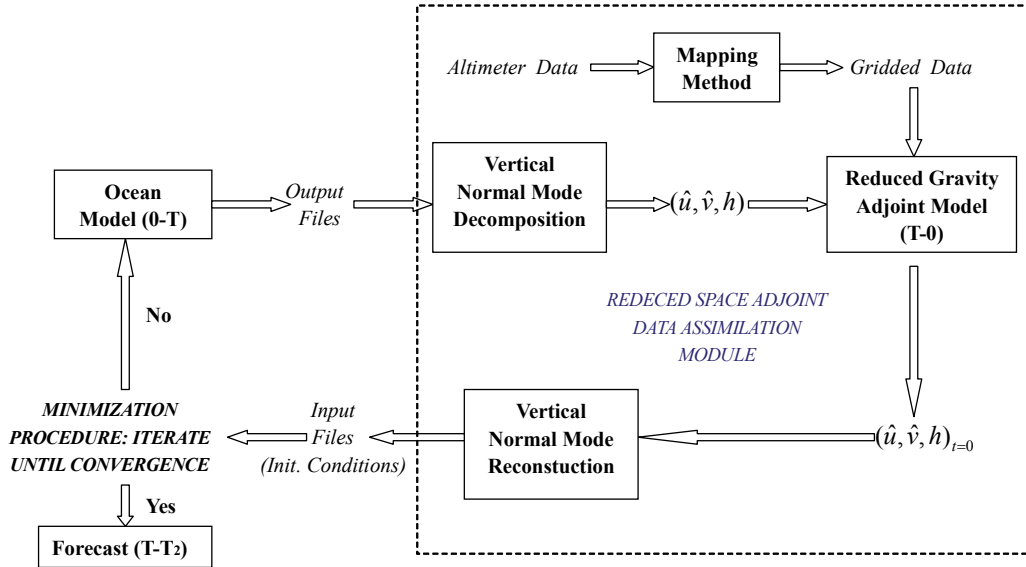


Figure 2.1. The flowchart of the reduced-space variational data assimilation technique. The models are run for the assimilation window $t=[0, T]$, and the forward model solution at time $t=T$ can be used to initialize a forecast.

2.2 Vertical Normal Mode Decomposition

Vertical normal mode decomposition is applied to retrieve the information from the forward ocean model and connect the forward and adjoint models which have different dynamics. The vertical normal modes are determined by solving the Sturm-Liouville type of partial differential equation:

$$S_{zz} + \frac{N^2}{gh} S = 0 \quad (2.1)$$

with boundary conditions:

$$S = 0, \quad \text{at } z = z_{bottom}, \quad (2.2)$$

$$S - hS_z = 0, \quad \text{at } z = 0 \quad (2.3)$$

(see Appendix A for the detailed derivation of 2.1-2.3), where S is a function of z , N is the Brunt-Väisälä frequency, g is the acceleration of gravity, and h is the equivalent depth.

Discretization of (2.1-2.3) yields an eigenvalue problem:

$$AS = \lambda S,$$

where A is an $n \times n$ tri-diagonal matrix, λ is the eigenvalue, and S is the eigenvector. The first eigenmode, called mode zero, is barotropic and all the other modes are baroclinic. Based on the magnitude of the eigenvalues, the baroclinic modes are ordered as mode one, mode two, etc. The mode number m is the number of zero-crossing(s) of the eigenvector R_m (Figure 2.2).

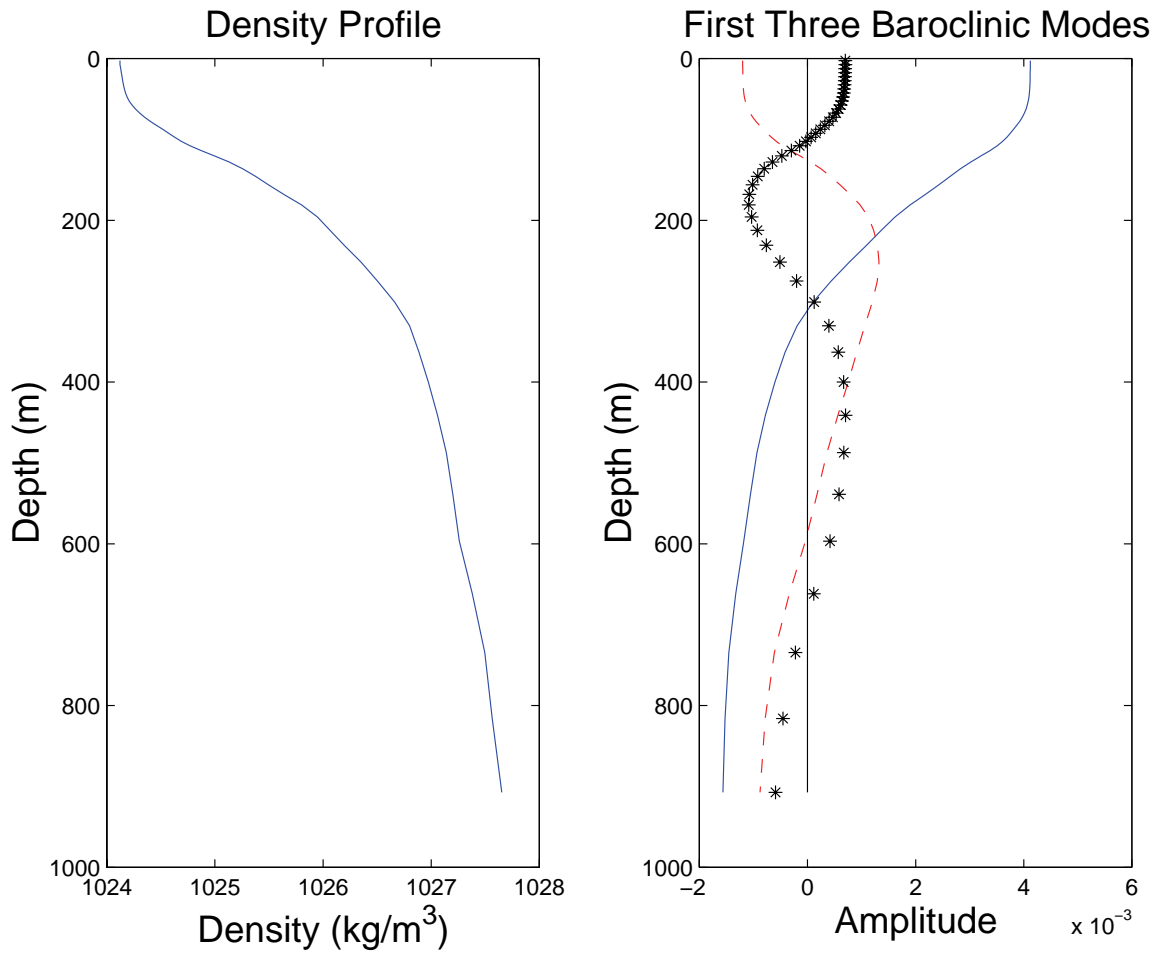


Figure 2.2. The density profile to which vertical normal mode decomposition is applied. Right: Eigenvectors R associated with the first three baroclinic modes. Blue solid line: mode one; Red dashed line: mode two; Black dotted line: mode three.

The eigenvectors R_m and S_m give the vertical structure of each mode, and the equivalent depth associated with each mode is obtained from the corresponding eigenvalue. Once the vertical normal modes are known, the complete three-dimensional time-dependent fields can be reconstructed as

$$u = \sum_{m=0}^M U_m(x, y, t) R_m(z), \quad (2.4)$$

$$v = \sum_{m=0}^M V_m(x, y, t) R_m(z), \quad (2.5)$$

$$\frac{p}{g\rho_0} = \sum_{m=0}^M \eta_m(x, y, t) R_m(z), \quad (2.6)$$

$$w = \sum_{m=0}^M W_m(x, y, t) S_m(z). \quad (2.7)$$

Suppose at the end of each iteration, the updates of the first baroclinic mode variables are ΔU_1 , ΔV_1 , and $\Delta \eta_1$. Since only the first baroclinic mode part of the field is updated and the separation of variables is linear, the update for the two horizontal velocity components and the pressure field are in the form of

$$u^{i+1}(x, y, z, 0) = u^i(x, y, z, 0) + \Delta U_1(x, y, 0) R_1(z), \quad (2.8)$$

$$v^{i+1}(x, y, z, 0) = v^i(x, y, z, 0) + \Delta V_1(x, y, 0) R_1(z), \quad (2.9)$$

$$p^{i+1}(x, y, z, 0) = p^i(x, y, z, 0) + g\rho_0 \Delta \eta_1(x, y, 0) R_1(z), \quad (2.10)$$

based on (2.4-2.6), where i is the iteration number.

Differentiating (2.10) with respect to z , one gets

$$p_z^{i+1}(x, y, z, 0) = p_z^i(x, y, z, 0) + g\rho_0\Delta\eta_1(x, y, 0)\frac{dR_1(z)}{dz}. \quad (2.11)$$

From (10A), the hydrostatic balance, the density update is

$$\rho^{i+1}(x, y, z, 0) = \rho^i(x, y, z, 0) - \rho_0\Delta\eta_1(x, y, 0)\frac{dR_1(z)}{dz}. \quad (2.12)$$

The updated density must then be converted to temperature and salinity variables for the forward model. For the application of the method used in this research, a mapping from density onto temperature and salinity is derived from the local temperature and salinity profile of the forward model as follows. At each grid point, the local vertical density, temperature, and salinity profiles averaged over time are obtained from the previous model run and hence the relation of these three variables is derived using the regression method. The update of the temperature and salinity variables is based on this relation and the density values. A quality control procedure is conducted after this, since some non-realistic values may occur over some points because of overshooting. An extreme value is replaced with the weighting average of the values from its neighboring points. Other techniques could also be used for the temperature and salinity update.

2.3 Numerical Optimization

The efficient implementation of the variational assimilation method depends crucially upon the fast convergence of a large-scale unconstrained minimization algorithm. Since problems in oceanography contain many degrees of freedom, the Limited Memory Quasi-Newton method (LMQN) (Navon and Legler, 1987; Navon *et al.*, 1992) is a good choice. A review of experiences and details concerning various

algorithms can be found in Zou *et al.* (1993). In the LMQN algorithm, the optimal solution is approximated asymptotically by adjusting the value of the control variables iteratively along its gradient or a direction obtained from a combination of the gradients from previous iterations.

Assume that \mathbf{g}_k ($\mathbf{g}_k = g(\mathbf{x}_k) = \nabla J(\mathbf{x}_k)$) is the gradient of the cost function with respect to the model control variables of the k th iteration, the LMQN method forms an approximation to the search direction, \mathbf{d}_k , which is defined as

$$\mathbf{d}_k = -\mathbf{H}_k \mathbf{g}_k \quad (2.13)$$

where \mathbf{H}_k is the inverse of the Hessian matrix (the second derivative of the cost function with respect to the control variables) of the k th iteration. A step size α_k along the descent direction \mathbf{d}_k is found, which satisfies

$$J(\mathbf{x}_k + \alpha_k \mathbf{d}_k) = \min_{\alpha} J(\mathbf{x}_k + \alpha \mathbf{d}_k), \quad (2.14)$$

and the control variables are updated using the formula

$$\mathbf{x}_{k+1} = \mathbf{x}_k + \alpha_k \mathbf{d}_k. \quad (2.15)$$

This procedure continues until the convergence criterion

$$\|\mathbf{g}_{k+1}\| \leq \varepsilon \max\{1, \|\mathbf{x}_{k+1}\|\} \quad (2.16)$$

is reached. Various LMQN methods differ in the choice of initial Hessian matrix \mathbf{H}_0 ,

the method computing $\mathbf{H}_k \mathbf{g}_k$, and the line search implementation that determines the suboptimal step size α_k . For the purpose of this study, the L-BFGS method (Liu and Nocedal, 1989) is used.

2.4 TOPEX/Poseidon and Jason-1 Altimeter Data

Many earth-observing satellites launched over recent years have provided scientists a huge amount of data. One such instrument important to oceanographers is the satellite altimeter. Satellite altimeters use microwave radar to determine the instantaneous elevation of the sea surface relative to an Earth-centered coordinate system, providing an absolute-reference frame for studies of sea level rise. Satellite altimeters provide frequent near-global data coverage of the world's oceans. This allows altimeter-derived estimates of the SSH to be based on data collected over most of the ocean surface in contrast to the conventional datasets, *e.g.*, the geographically sparse coastal data provided by tide gauges. Data from the T/P and Jason-1 satellite altimeters are chosen to be assimilated in this research.

The T/P satellite altimeter provided SSH measurements with a root mean square error of less than five centimeters from its launch in August 1992 until its failure in October 2005. The satellite had a 10-day repeat orbit, with 6.2 kilometers between observations along the ground track, and a 315-kilometer distance between neighboring ground tracks at the equator. A complete cycle in the data record consists of 127 orbits and each orbit has a period of 112 minutes.

Jason-1, a follow-on to the T/P mission with similar functions, was launched on December 2001. After a period of flying in tandem with T/P, T/P was commanded to move onto a parallel ground track mid-way between two adjacent Jason-1 ground tracks.

With the addition of this new satellite, the spatial coverage of the observations doubled for the period during which both instruments operated.

Despite the increased spatial coverage provided by the two orbiting altimeters (Figure 2.3), there are still large gaps between the ground tracks comparable to mesoscale oceanic features. For example, oceanic eddies have measurable sea level anomalies and diameters of roughly 100 kilometers. Loop Current eddies in the Gulf of Mexico are large (typically 150 to 200 kilometers) anticyclones with anomalously high sea levels in the center, commonly over 50 centimeters. These, along with cyclonic eddies and some smaller features, generally propagate toward the west. While observing these eddies with T/P and Jason-1 data, major difficulties arise when the centers of these eddies are located between satellite ground tracks. Traditional spatial interpolation of these satellite data will result in intermittent occurrences of these eddies in spatial maps of SSH constructed from T/P and Jason-1 data. As a consequence, it is necessary to use a good interpolation procedure to create a regular set of data values as part of the data processing.

2.5 Mapping Satellite Altimeter Data

During the course of this research, a mapping technique (Yu *et al.*, 2004) has been developed to produce an SSH data set with a regular temporal and spatial grid for assimilation. The mapping method considers not only the observations within the assimilation cycle but also those prior to the assimilation window. This allows a shorter assimilation cycle, since the technique maps the original observations from satellite ground track observational locations onto a finer spatial and temporal grid and hence reduces the time for the propagation of information between the grid points. This method is based on complex empirical orthogonal function (CEOF) analysis (Barnett, 1983; Shriver *et al.*, 1991). CEOF analysis extracts physical information on propagating

T/P and Jason 1 ground tracks in the Gulf of Mexico

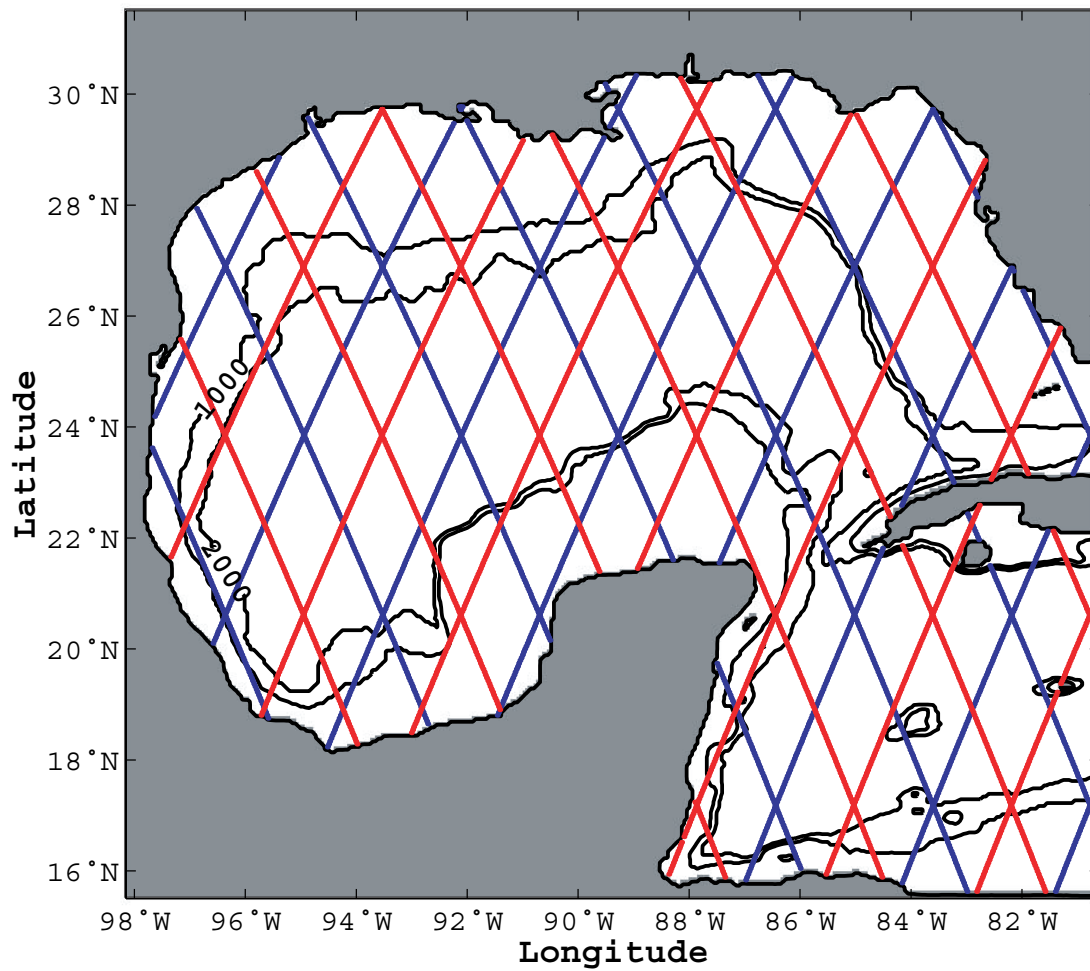


Figure 2.3. The TOPEX/Poseidon and Jason-1 ground tracks in the Gulf of Mexico. Red lines: T/P ground tracks; blue lines: Jason-1 ground tracks.

features from a two-dimensional data array,

$$D = (h_{nm})_{N \times M}, \quad (2.17)$$

where D is an $N \times M$ matrix with elements h_{nm} , and N and M are the numbers of space and time points, respectively. With the use of CEOF analysis the component eigenmodes of D are obtained.

From the CEOF component eigenmodes of D , M pairs of complex vectors T_i and S_i , are determined as

$$T_i = (T_m)_{1 \times M}, \quad (2.18)$$

$$S_i = (S_n)_{N \times 1}. \quad (2.19)$$

The vector S will be referred to as the spatial function (SF) and T as the temporal function (TF). By definition a complex vector $C(x)$ can be represented as

$$C(x) = A(x) \exp[i\Theta(x)] \quad (2.20)$$

where $A(x)$ is an amplitude and $\Theta(x)$ is a phase, which can also be rewritten as

$$S(x) = E(x) \exp[i\Theta(x)], \quad (2.21)$$

$$T(t) = R(t) \exp[i\phi(t)]. \quad (2.22)$$

Their product (real part) is

$$\text{Re}\{E(x)R(t)\exp[i(\Theta(x) + \phi(t))]\} = E(x)R(t)\cos(\Theta(x) + \phi(t)). \quad (2.23)$$

$E(x)$ (the spatial amplitude function) shows the variability of the amplitude in space associated with a given eigenmode. $R(t)$ (the temporal amplitude function) provides the information on the variability of the amplitude in time. For a line of constant phase (letting $\xi(x, t) = \Theta(x) + \phi(t)$),

$$d\xi(x, t) = \frac{\partial\Theta(x)}{\partial x} dx + \frac{\partial\phi(t)}{\partial t} dt = 0, \quad (2.24)$$

or rearranging,

$$\frac{\partial x}{\partial t} = c = -\frac{\partial\phi(t)/\partial t}{\partial\Theta(x)/\partial x}. \quad (2.25)$$

The phase speed is $c = \omega/k$, where

$$k = \frac{\partial\Theta(x)}{\partial x}, \quad (2.26)$$

$$\omega = -\frac{\partial\phi(t)}{\partial t}. \quad (2.27)$$

CEOF analysis decomposes data into orthogonal modes, identifies the propagating information, and obtains the spatial and temporal information associated with each mode. The most significant modes (modes with larger eigenvalues compared to others) are chosen among all modes and contain most of the variability. For the TF and SF with respect to each mode, the phase and amplitude information is mapped onto a regular finer grid in time and/or space. From these remapped phase and amplitude functions, the

new TFs and SFs are rebuilt and the data set is reconstructed by summing the product of TF and SF associated with each mode.

As a demonstration, the method is tested with a simple analytical experiment requiring only the temporal interpolation. In this case, a sinusoidal wave is propagating to the right and is sampled at each one fourth of its period (*i.e.*, there are four observations, or samples, during each cycle). The result from a traditional interpolation method (linearly interpolate data in time between samples) is shown as a comparison with the result from the new mapping method (Figure 2.4). It is clear that the new method identifies the propagating information very well and retains the wave form and amplitude at the interpolated time much better than the linear interpolation method, which reduces the amplitude of the wave.

The second experiment simulates a more realistic scenario in order to demonstrate the spatial interpolation of this technique (Figure 2.5). In this experiment a synthetic eddy propagates to the left. The SSH field is sampled at locations simulating the orbiting T/P satellite altimeter observational pattern. The mapping method is applied and interpolates the synthetic along-track SSH observations onto a finer regular spatial grid. The reconstruction yields an SSH field very close to the “truth”. A closer look shows that the technique recovers the maximum successfully when the eddy moves to between tracks. This new mapping technique is applied to the T/P and Jason-1 satellite along-track data to produce an SSH data set regularly gridded in time and space for assimilation into the ocean model, as described in Chapter 3.

2.6 The Ocean Model

The model used to test the reduced-space variational data assimilation technique is the NCOM developed at the Naval Research Laboratory—Stennis Space Center (Martin,

2000; Morey *et al.*, 2003). It uses a hybrid sigma-z level coordinate. The free surface is a sigma level, and the levels below the free surface are a specified number of sigma and z-levels.

The NCOM is a fully three-dimensional primitive equation ocean model with the hydrostatic, incompressible, and Boussinesq approximations. The equations, in Cartesian coordinates, are

$$\frac{\partial u}{\partial t} = -\nabla \cdot (\mathbf{v}u) + Qu + fv - \frac{1}{\rho_0} \frac{\partial p}{\partial x} + F_u + \frac{\partial}{\partial z} (K_M \frac{\partial u}{\partial z}), \quad (2.28)$$

$$\frac{\partial v}{\partial t} = -\nabla \cdot (\mathbf{v}v) + Qv - fu - \frac{1}{\rho_0} \frac{\partial p}{\partial y} + F_v + \frac{\partial}{\partial z} (K_M \frac{\partial v}{\partial z}), \quad (2.29)$$

$$\frac{\partial p}{\partial z} = -\rho g, \quad (2.30)$$

$$\frac{\partial u}{\partial x} + \frac{\partial v}{\partial y} + \frac{\partial w}{\partial z} = Q, \quad (2.31)$$

$$\frac{\partial T}{\partial t} = -\nabla \cdot (\mathbf{v}T) + QT + \nabla_h (A_H \nabla_h T) + \frac{\partial}{\partial z} (K_H \frac{\partial T}{\partial z}) + Q_r \frac{\partial \gamma}{\partial z}, \quad (2.32)$$

$$\frac{\partial S}{\partial t} = -\nabla \cdot (\mathbf{v}S) + QS + \nabla_h (A_H \nabla_h S) + \frac{\partial}{\partial z} (K_H \frac{\partial S}{\partial z}), \quad (2.33)$$

$$\rho = \rho(T, S, z), \quad (2.34)$$

where t is the time, x , y , and z are the three coordinate directions, u , v , and w are the three components of the velocity, Q is a volume flux source term, \mathbf{v} is the vector velocity, T is the potential temperature, S is the salinity, ∇_h is the horizontal gradient operator, f is the Coriolis parameter, p is the pressure, ρ is the water density, ρ_0 is a reference water density, g is the acceleration of gravity, F_u and F_v are the horizontal mixing terms for momentum, A_H is the horizontal mixing coefficient for scalar fields (potential

temperature and salinity), K_M and K_H are the vertical eddy coefficients for momentum and scalar fields, respectively, Q_r is the solar radiation, and γ is a function describing the solar extinction.

The model supports a number of higher order numerical methods. For these simulations, a quasi-third-order advection scheme is used with a leapfrog time differencing scheme.

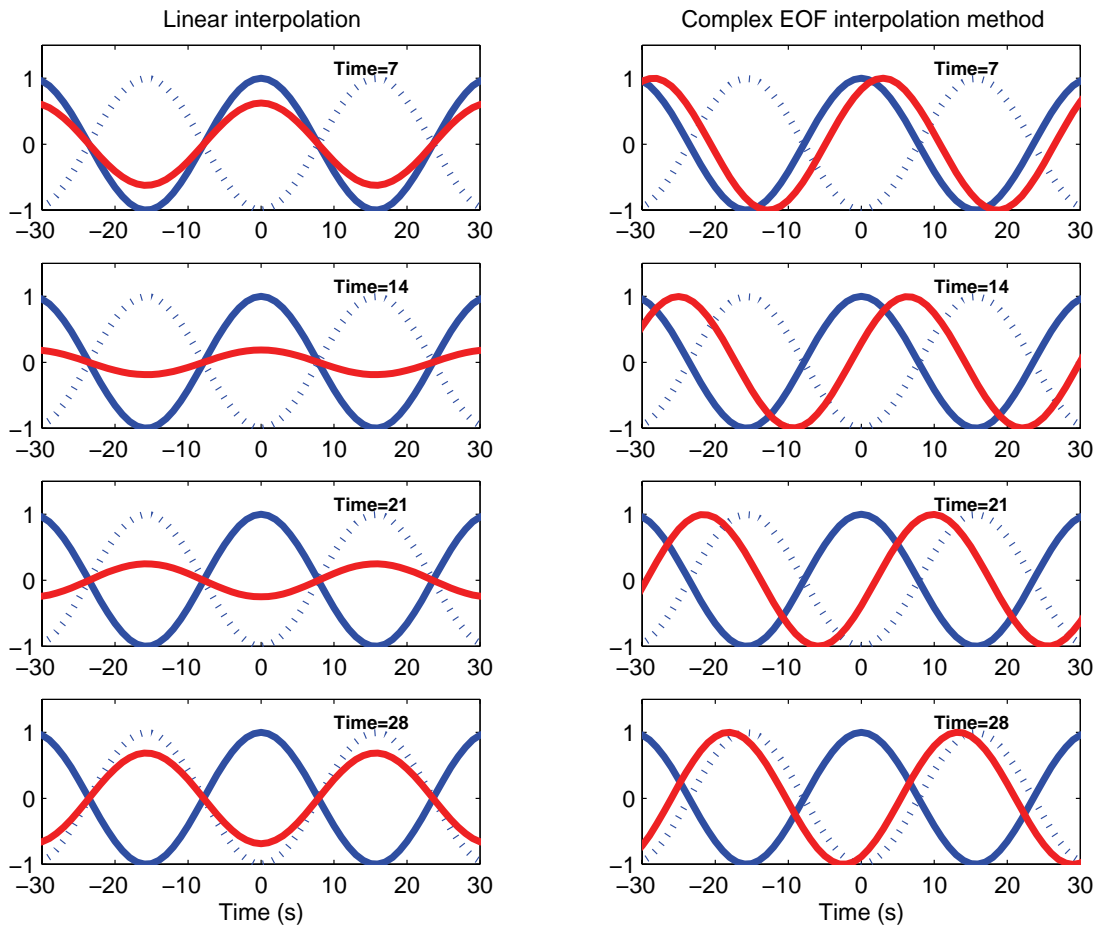


Figure 2.4. The interpolation of a sine wave propagating to the right. Positions shown are $t=0$ (blue) and $t=32$ (hatched). Interpolation results (red) at positions at $t=7, 14, 21, 28$ are shown. The left panels show results based on linear interpolation, and the right panel panels show results based on the new mapping method.

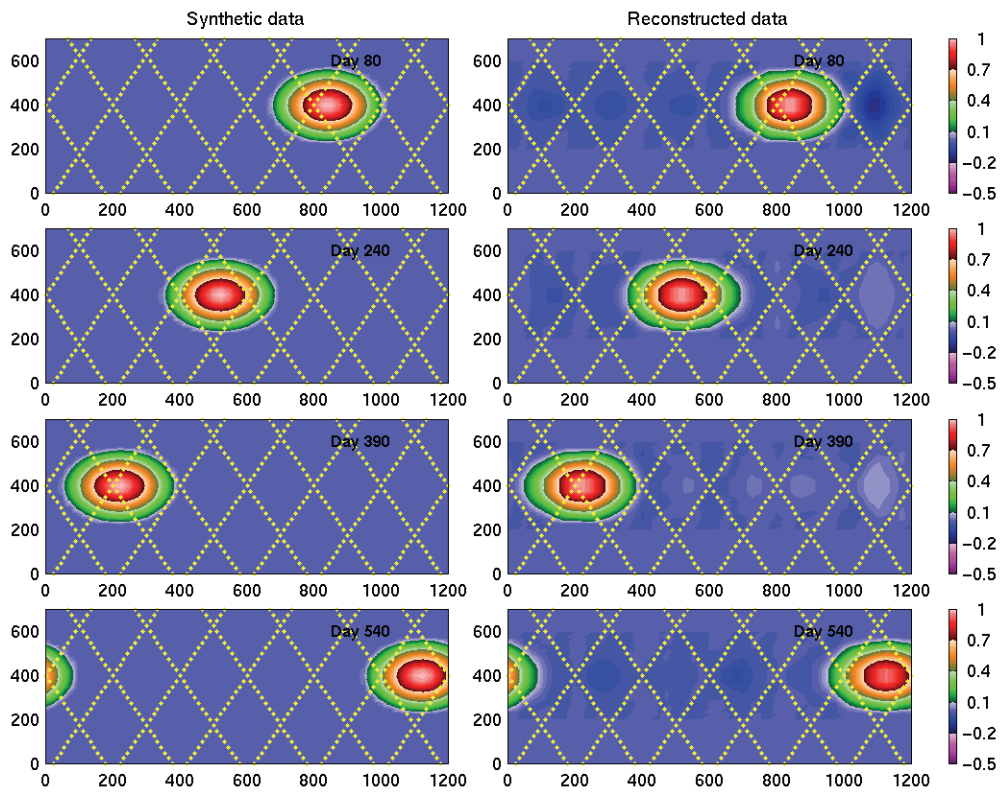


Figure 2.5. A synthetic eddy propagating westward (left) and the field produced by application of the CEOF mapping method (right) applied to simulated satellite “observations” at yellow dots.

3. EXPERIMENTS AND RESULTS

The reduced space variational data assimilation method, described in Chapter 2, is applied to an NCOM simulation of the Gulf of Mexico for testing and demonstration. Three numerical experiments are run. The first is an idealized experiment in that the data to be assimilated are not obtained from satellite altimetry, but are rather the SSH field from a model run. The data are then assimilated into a model that has started from a different initial state and the goal is to adjust the model initial state to the original one from which the assimilated SSH data are obtained. The second experiment is similar to the first, except that the SSH data are sampled along a pattern similar to the T/P and Jason-1 satellite tracks, and the mapping technique is applied to construct the gridded SSH fields to be assimilated. The last experiment is an application of the technique with real data, assimilating T/P and Jason-1 data from January 9, 2004 to January 18, 2004.

3.1 Idealized Experiment One

The data assimilation technique is tested using the NCOM configured for a domain covering the entire Gulf of Mexico and the northwestern Caribbean ($98.15^{\circ}\text{W} - 80.60^{\circ}\text{W}$, $15.55^{\circ}\text{N} - 31.50^{\circ}\text{N}$) (Figure 3.1). The horizontal resolution is 0.05° in both latitude and longitude and there are 352 grid points zonally and 320 grid points meridionally. It has 20 evenly spaced sigma levels above 100 m depth and 40 z-levels below 100 m with a maximum depth of 4000 m. Open boundaries are found along the eastern edge of the domain in the Caribbean and the Florida Straits. This model is integrated for a period

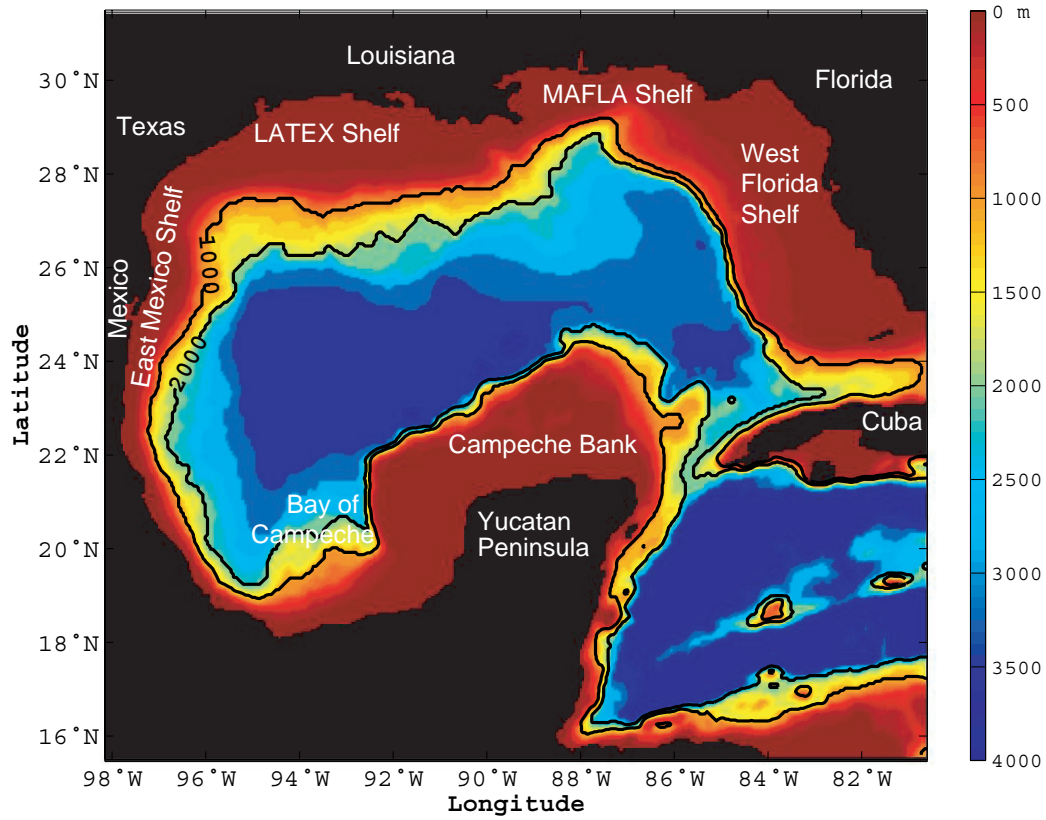


Figure 3.1. The model domain (98.15°W–80.60°W, 15.55°N–31.50°N) and topography for the NCOM simulations used in this work.

of 11 years from rest forced by wind stress, latent, sensible, and radiative heat fluxes derived from the *DaSilva et al.* (1994) $0.5^\circ \times 0.5^\circ$ analyzed COADS monthly climatology fields. The 1994 World Ocean Atlas (National Oceanic and Atmospheric Administration, 1994) (WOA94) is used to derive the model initial temperature and salinity fields.

The model fields at the end of the 11th year are used as the initial condition for the first iteration of the assimilation technique (a “first guess”). The NCOM is then integrated with a different initial condition as a control or truth run. The SSH field at the native model resolution is sampled at one-day time intervals as the “observation” fields (Figure 3.2). The goal of this experiment is to assimilate the SSH data from the truth run into the model to adjust it toward the same state as the truth run. This experiment assimilates an SSH observation field into a model that has not been constrained to match the truth fields in any way. Thus, the first guess is quite different from the observation. The purpose is to illustrate how the technique works and show if it can handle a bad first guess of the initial condition.

During each iteration the NCOM is run from an initial condition for a ten-day period and the cost function, defined as in Appendix B, is calculated. Vertical normal mode decomposition is applied to retrieve the first baroclinic mode SSH and horizontal velocity fields as the model control variables and to get the eigenfunction corresponding to the first baroclinic mode. The adjoint model is integrated backward in time for ten days to obtain the gradient of the cost function with respect to the model control variables. The L-BFGS method (the details are in Chapter 2) is applied to minimize the cost function and update the first baroclinic mode SSH and horizontal velocity fields at the model initial time. These updated first baroclinic mode variables are used to calculate the update for the full model velocity and pressure fields through vertical normal mode reconstruction. The density, temperature, and salinity are updated based on the algorithm described in Chapter 2. The whole procedure repeats until a prescribed convergence criterion is met.

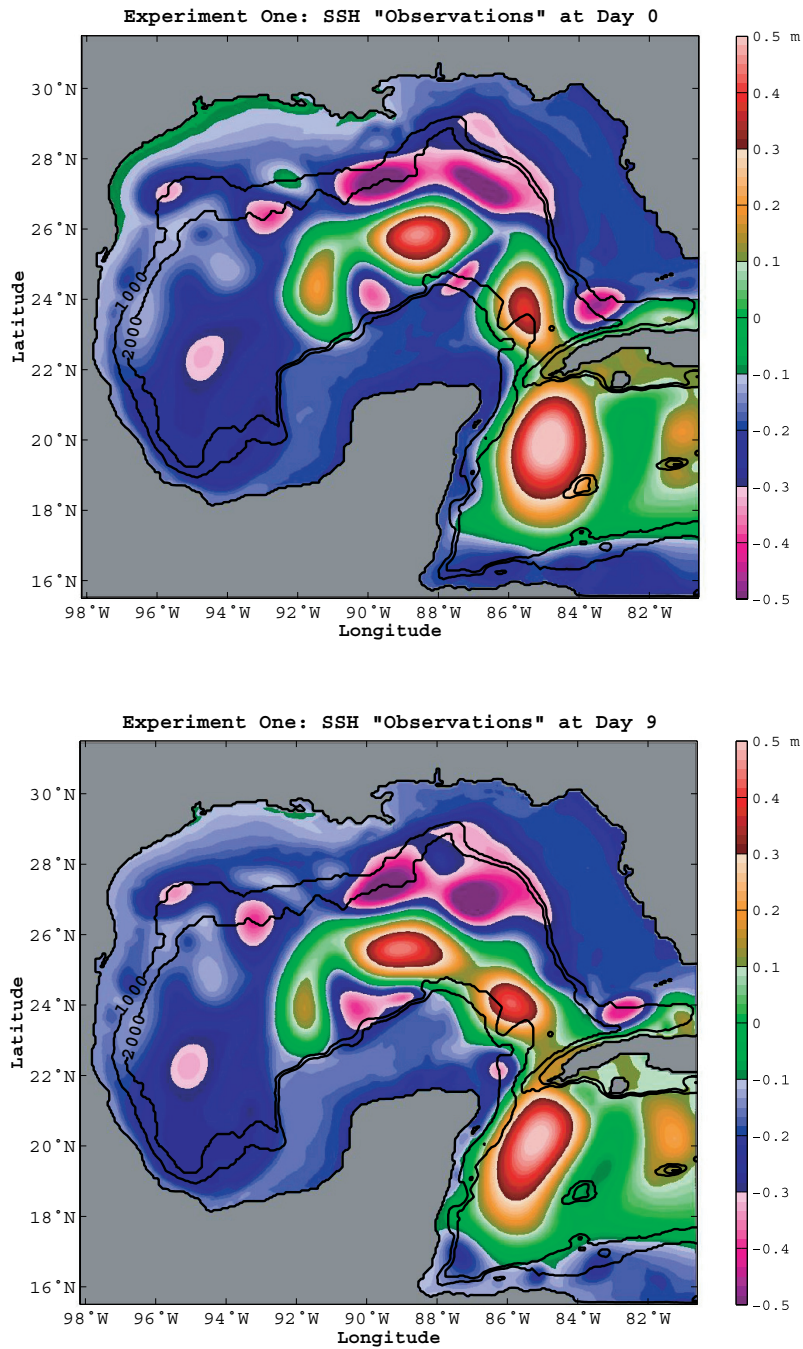


Figure 3.2. The SSH fields from the model control run in idealized experiment one (used as “observations”) at model day 0 (top) and model day 9 (bottom).

The cost function normalized by its value of the first iteration (Figure 3.3a) does not decrease dramatically during the first three iterations, and then drops rapidly in the following several iterations when the optimization algorithm gathers more information from the previous iterations. By iteration 7, it drops to 17% of the value from the first iteration with negligible change following subsequent iterations. The evolution of the gradient norm normalized by its value from the first iteration is similar to that of the cost function (Figure 3.3b). Since the system is based on several assumptions, it is reasonable to have a non-monotonically decreasing cost function (more details of this will be given in the following chapter).

The SSH field (Figure 3.4) is effectively adjusted by the assimilation technique and reaches a state that is closer to the observation field. The biggest difference between the first guess and the observation is the big anticyclonic eddy in the northwestern Gulf of Mexico. It disappears after the assimilation procedure and the SSH field in the area around Cuba improves dramatically. The root mean square error (RMSE, which is defined in the form of $\sqrt{\overline{(SSH(x, y, t) - SSH_{obs}(x, y, t))^2}}$, where $\overline{\quad}$ means a time average over the assimilation window) fields (Figure 3.5) supply a better comparison. The RMSE averaged over the model domain, defined in a way equivalent to the square root of the cost function, behaves in a similar way as the cost function. The 18°C isotherm map (Figure 3.6) indicates that vertical normal mode decomposition and reconstruction effectively transfers the information observed at the sea surface to deep layers. Since the adjoint model has only one vertical layer due to the simplified dynamics, it takes much less time (around 1/30 of the computational time required by the NCOM) than the forward model run.

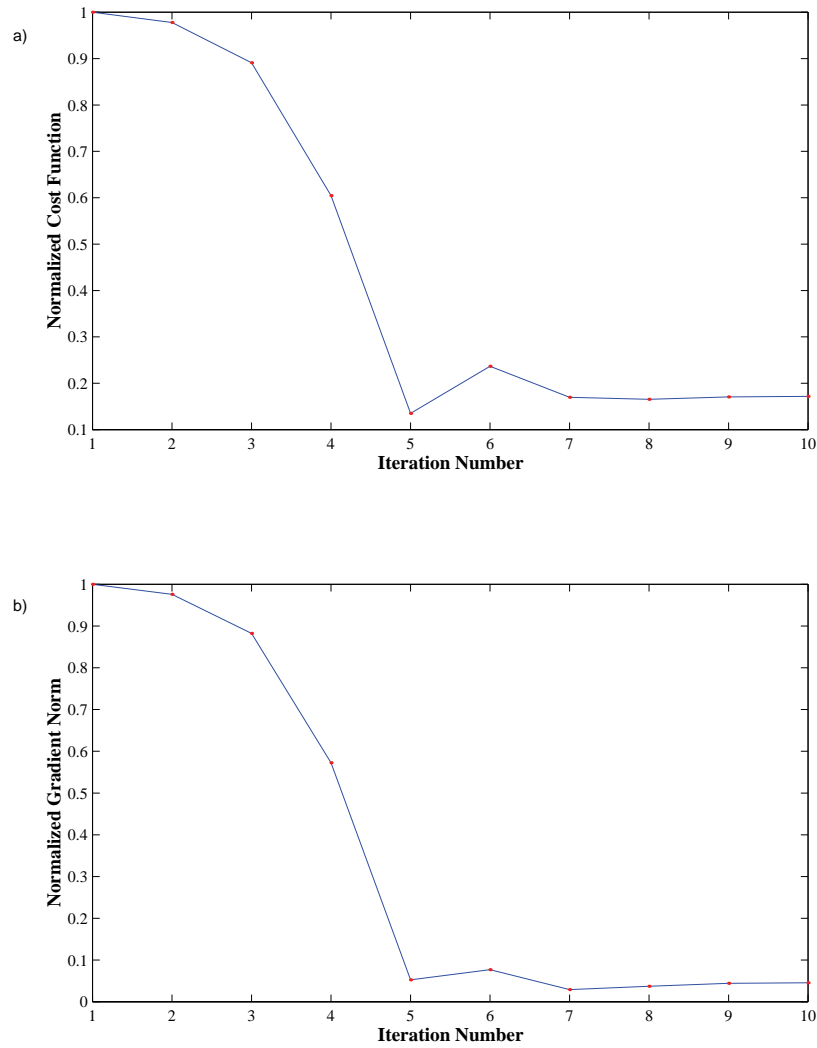


Figure 3.3. The normalized cost function (top) and the normalized gradient norm (bottom) with respect to the iteration number in experiment one.

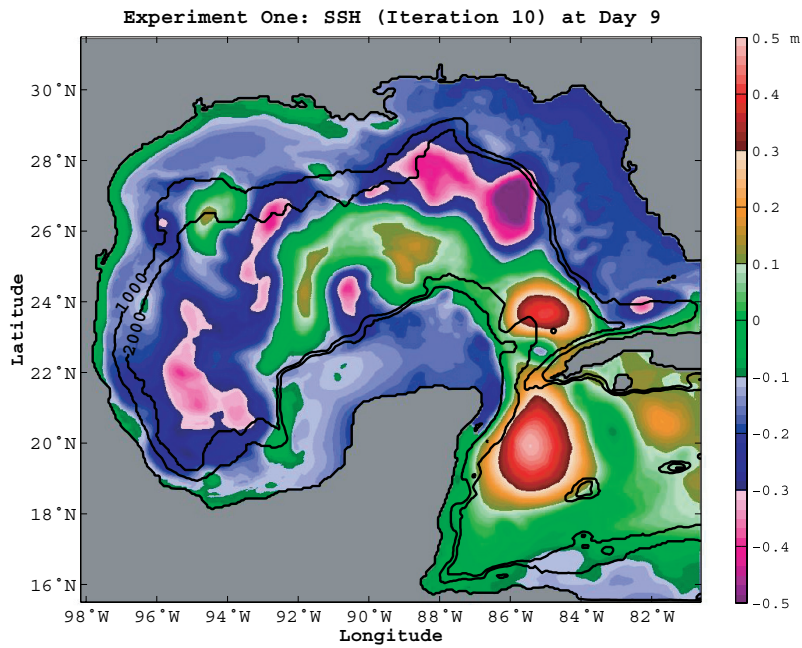
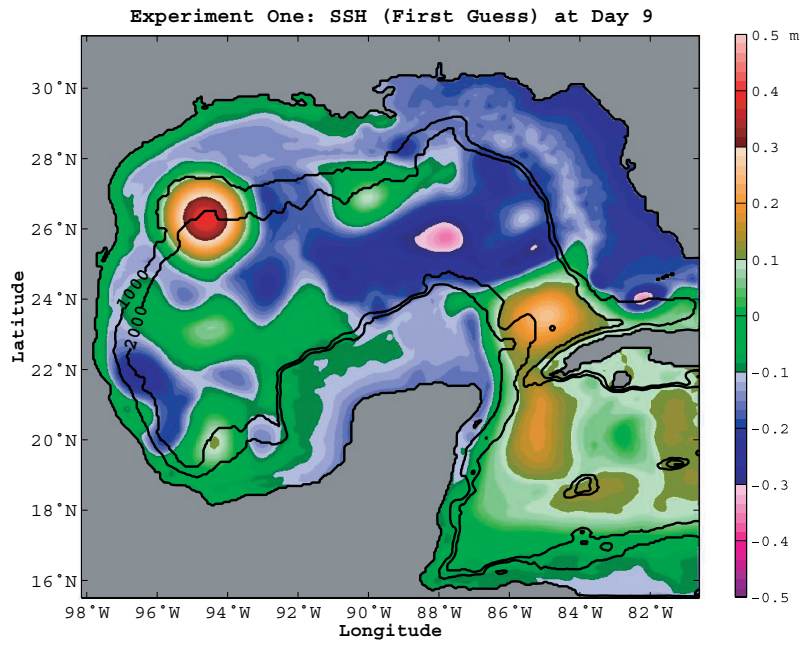


Figure 3.4. SSH synoptic maps (at model day 9) of the initial guess (top) and iteration 10 (bottom).

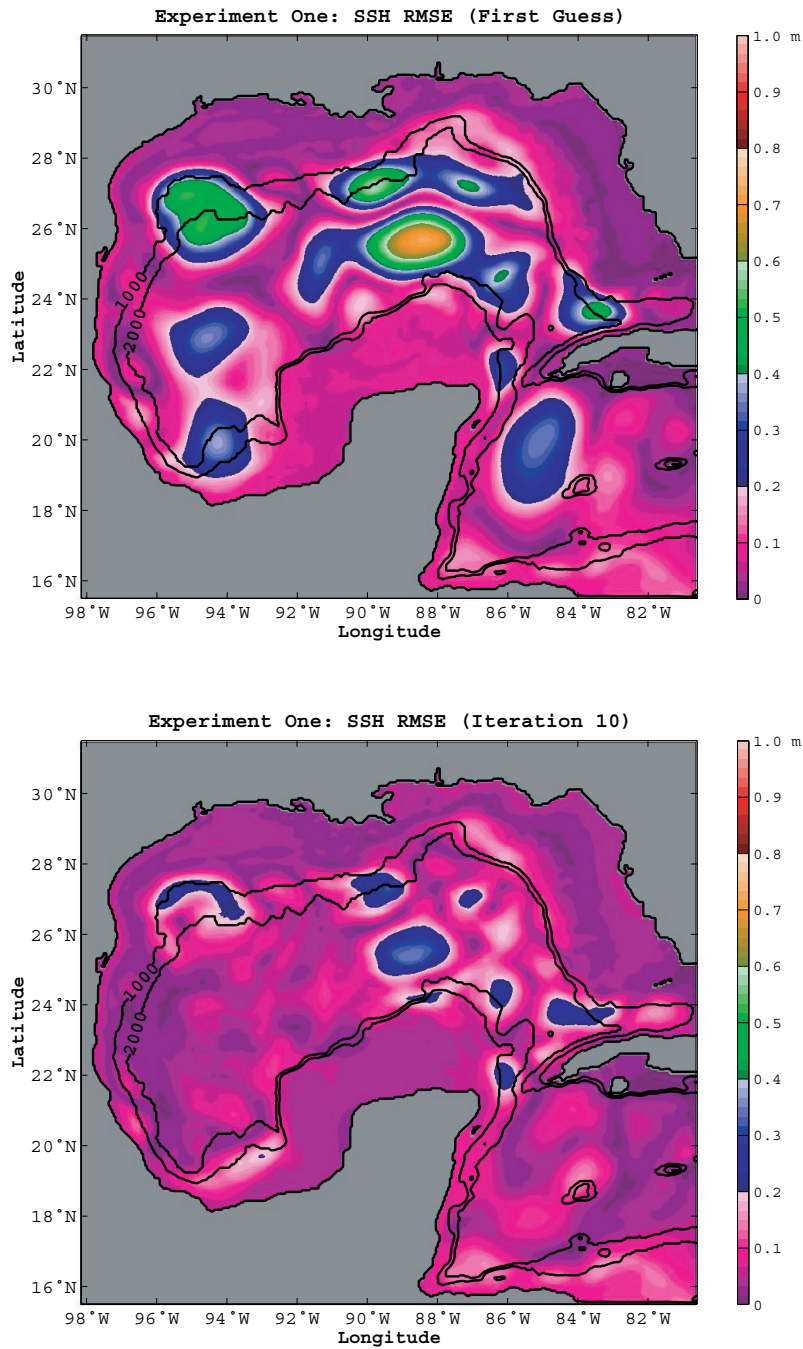


Figure 3.5. The root mean square error (RMSE) of SSH of the initial guess (top) and iteration 10 (bottom) computed from the control run SSH fields.

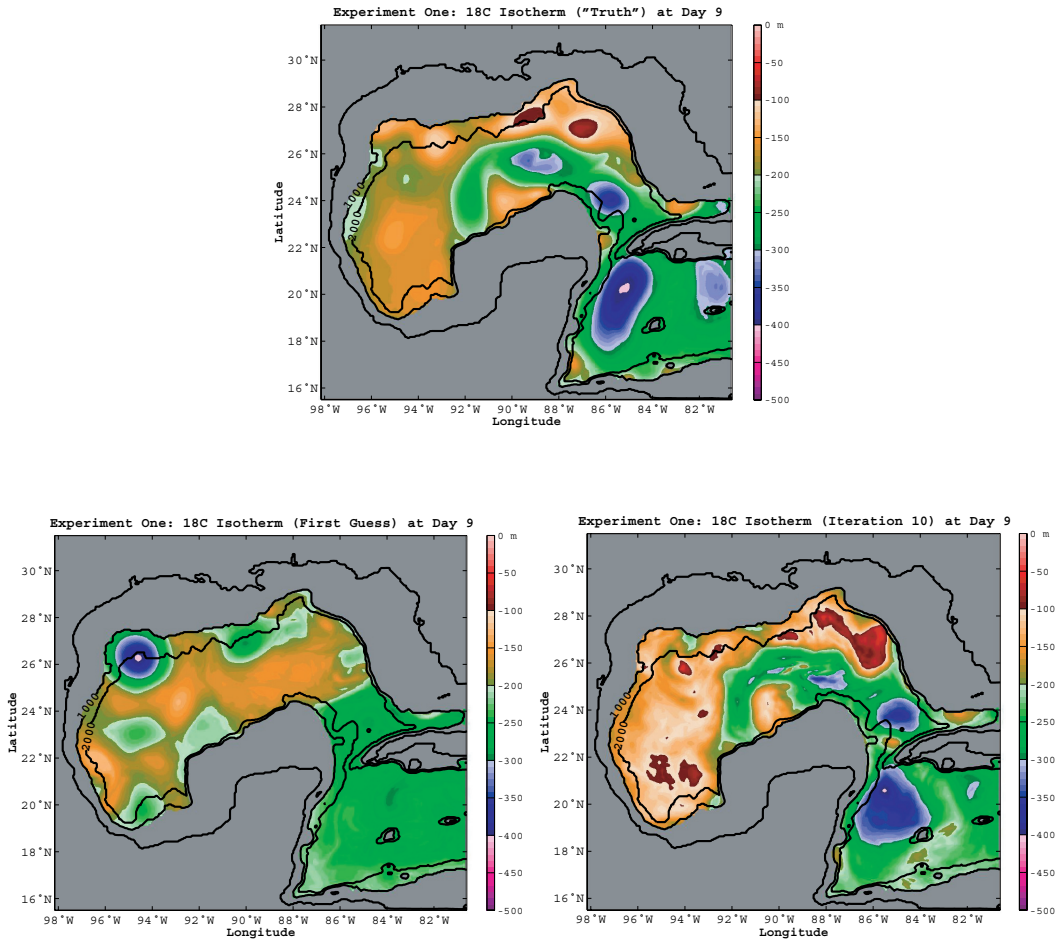


Figure 3.6. The 18°C isotherm depth (at model day 9) of the “truth”, or control run (top), the first guess (lower left) and iteration 10 (lower right).

3.2 Idealized Experiment Two

This experiment is designed to simulate a more realistic scenario in which the SSH is sparsely sampled by satellite altimeters. The model configuration is the same as in experiment one. After the eleven-year spin-up period the NCOM is run for an additional 100 days. Rather than assimilating the SSH field with the native model grid, the model SSH data are sampled along locations corresponding to T/P and Jason-1 observation locations every ten days. The mapping technique, described in Chapter 2, is applied to interpolate the data to the native model grid in space and to a one-day interval over time between day 90 and day 99 as the observations. The comparison between the mapped SSH data and the model truth SSH fields (Figure 3.7) shows that the gridded SSH constructed from the mapping method represents the original field well.

The NCOM model state at the end of the 11-year spin-up period (before the additional 100 days of integration) is taken as the first guess of the assimilation and the same assimilation procedure is applied. Thus, the first guess is a perturbation from the truth as they are separated in time by 90 days. The cost function reaches 36% of its value at the first iteration after iteration six with a rapid reduction of the cost function and the normalized gradient norm during the first four iterations (Figure 3.8). The comparison between the truth and the NCOM outputs (Figure 3.9) shows the improvement of the SSH field during the assimilation, *e.g.*, the shape of the large anticyclonic eddy in the northwestern Gulf is closer to the truth; the positions and shapes of the eddies at Bay of Campeche are improved; and the shedding of an anticyclonic eddy at the end of the assimilation window is recovered. The surface velocity field is also dynamically consistent with the SSH field. The SSH RMSE (Figure 3.10) gives a clearer comparison between the truth and the model outputs. Two 10-day forecasts are conducted in order to show the impact of the assimilation on forecasting. The first one takes the model state of the first guess at day 9 as the initial condition and the second one takes that of iteration 13 at day 9 as the initial condition. The SSH RMSE (Figure 3.11) of these two

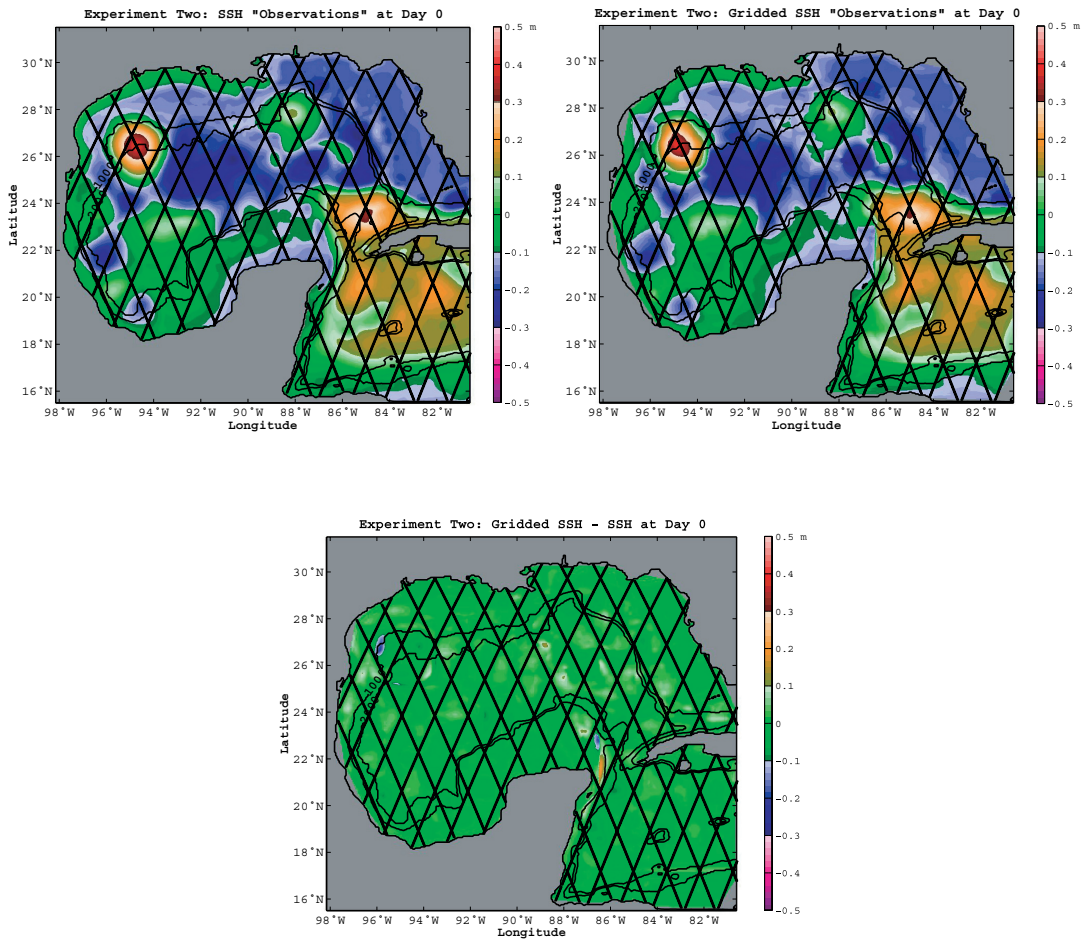


Figure 3.7. (a) Top left: Control run (“truth”) SSH field from experiment two. Top right: SSH field constructed by applying the CEOF mapping technique to values sampled along locations corresponding to T/P and Jason-1 observation locations (black dots) every ten days. Bottom: Difference between the two SSH fields. All fields are from model day 0.

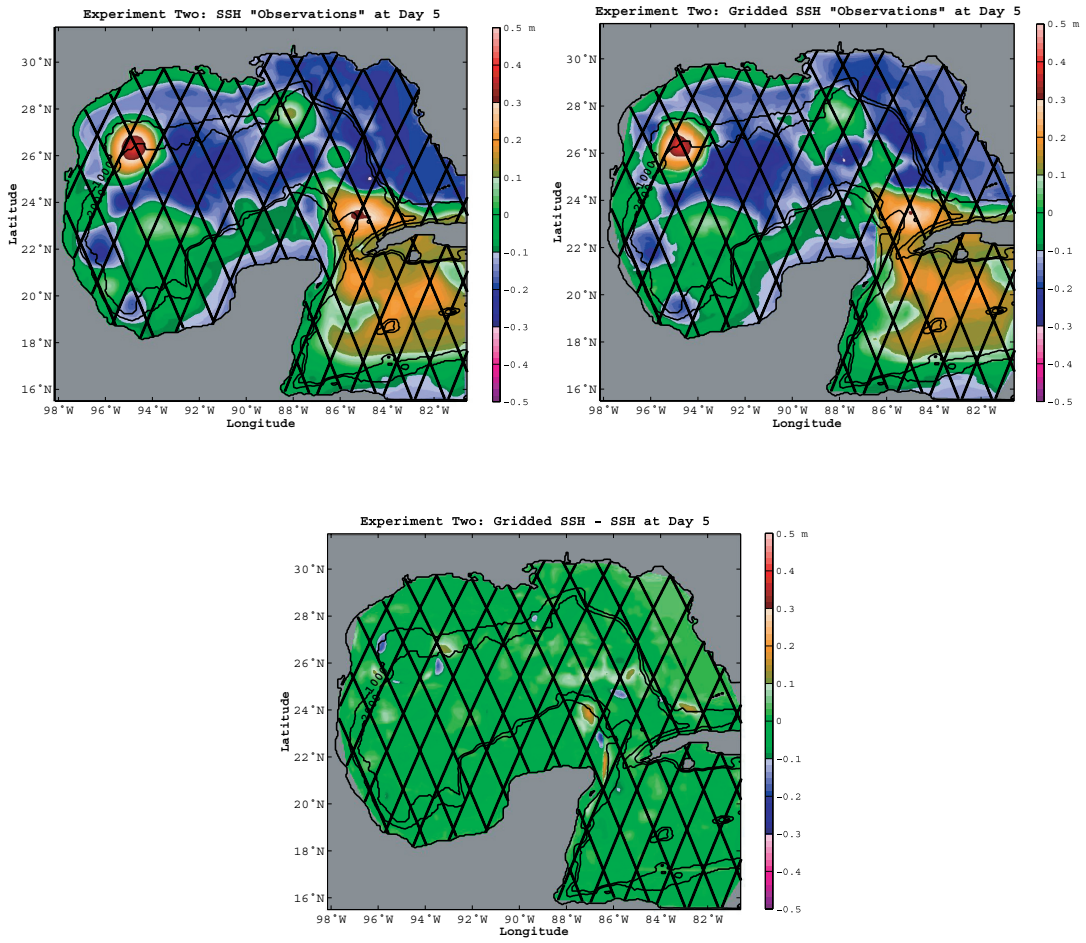


Figure 3.7. (b) Same as Figure 3.7(a) except that the results at model day 5 are shown.

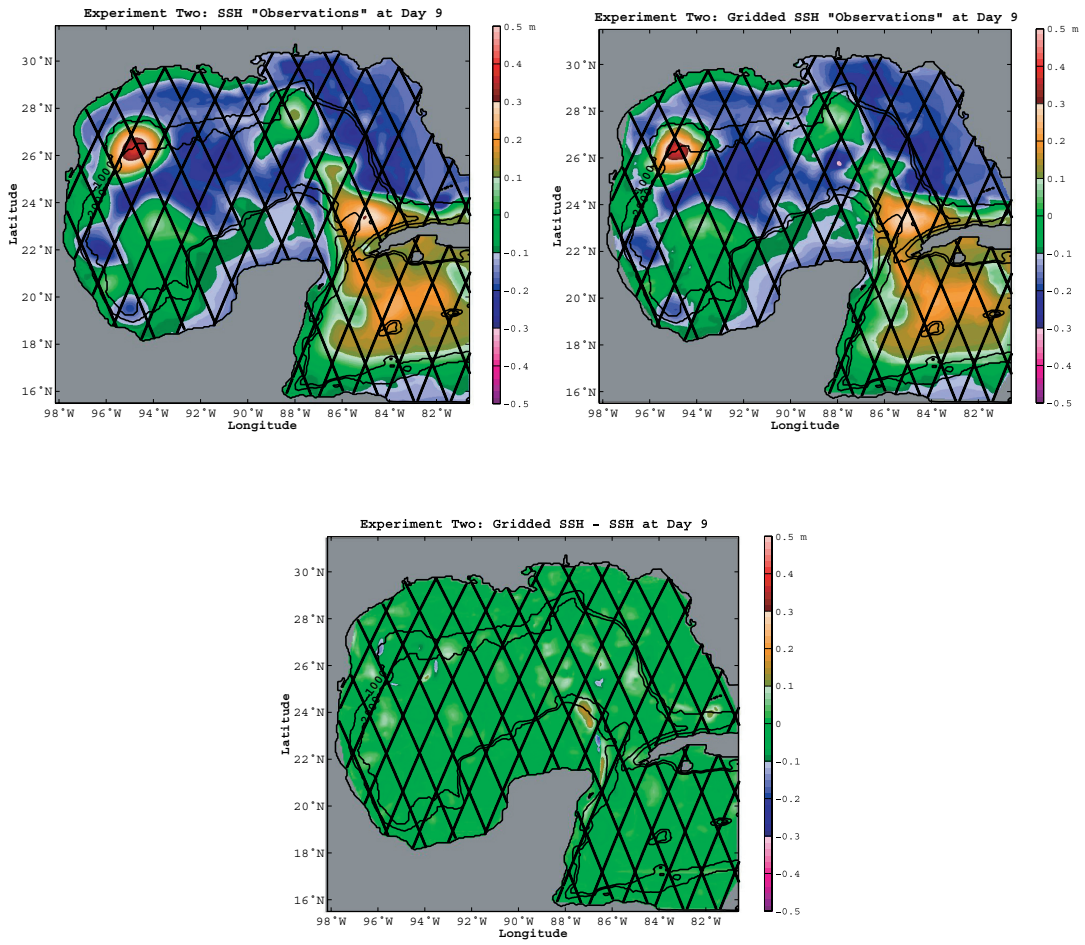


Figure 3.7. (c) Same as Figure 3.7(a) except that the results at model day 9 are shown.

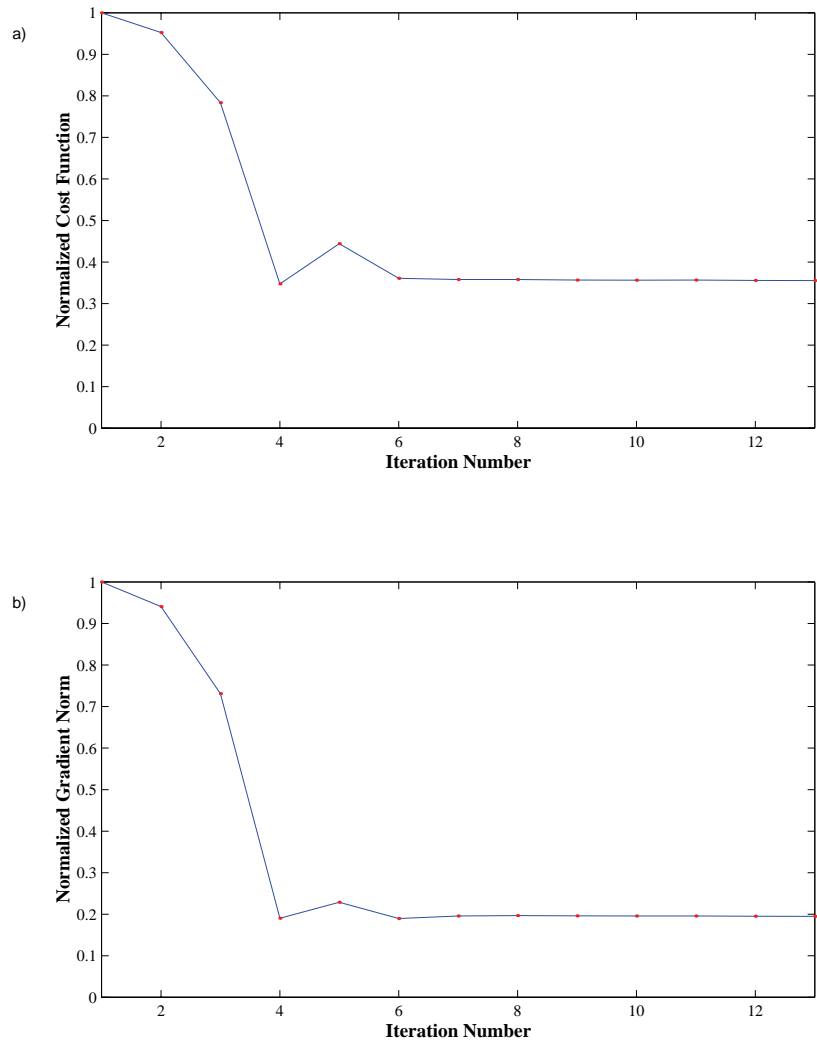
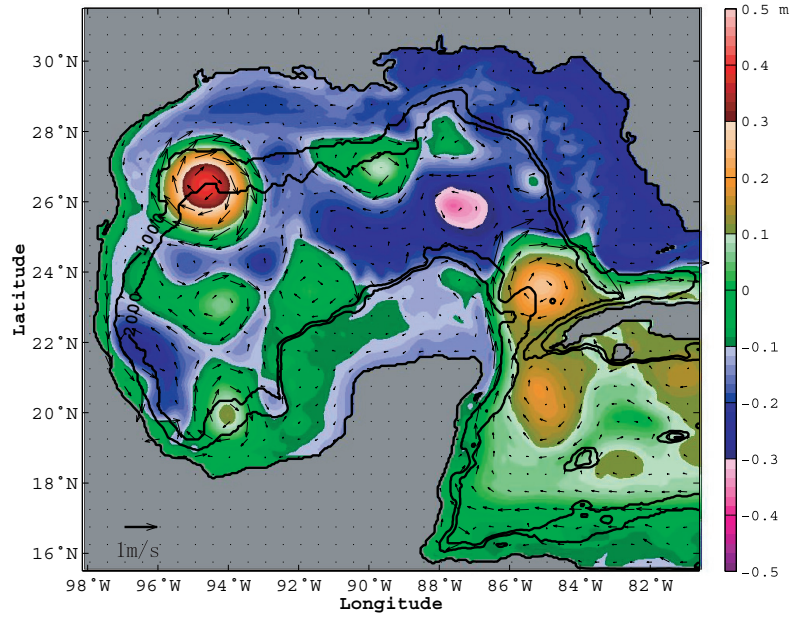


Figure 3.8. The normalized cost function (top) and the normalized gradient norm (bottom) with respect to iteration number for experiment two.

Experiment Two: SSH and Surface Velocity (First Guess) at Day 0



Experiment Two: SSH and Surface Velocity (First Guess) at Day 9

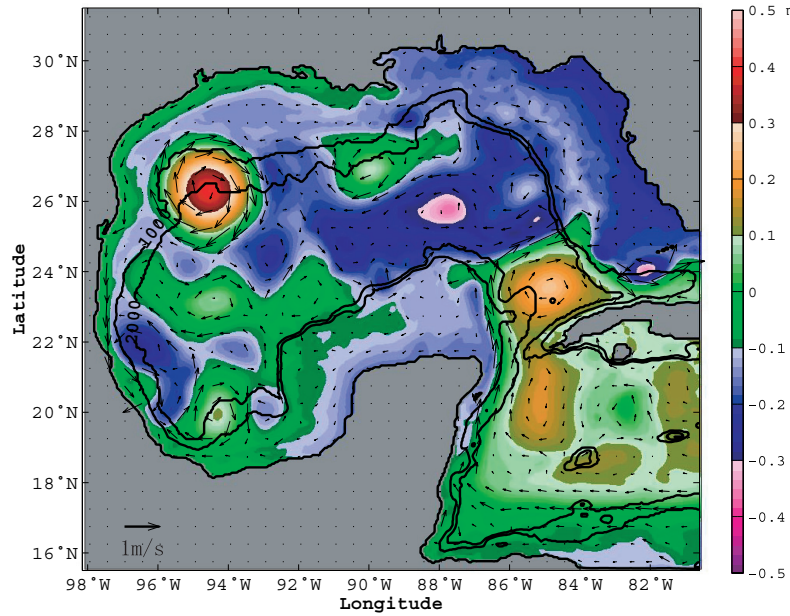
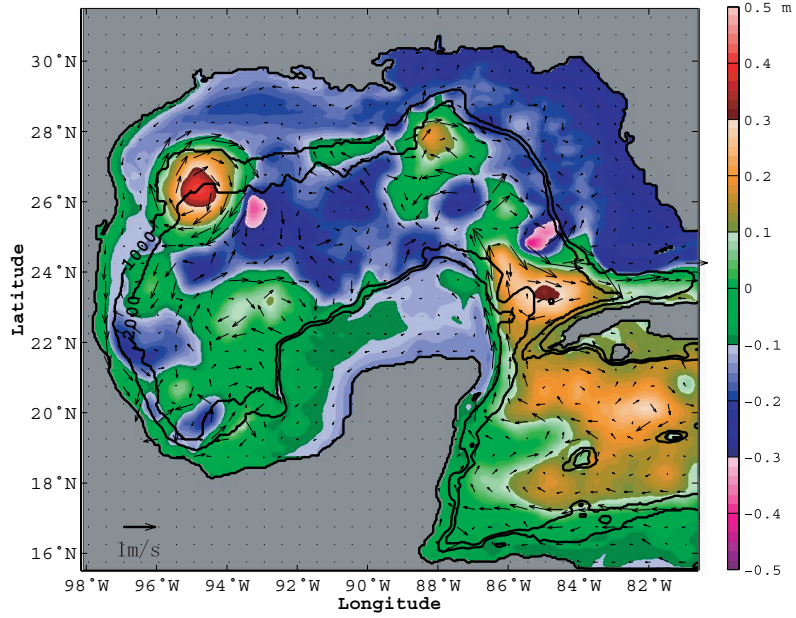


Figure 3.9. (a) The SSH and surface velocity synoptic maps of the initial guess at model day 0 (top) and model day 9 (bottom).

Experiment Two: SSH and Surface Velocity (Iteration 13) at Day 0



Experiment Two: SSH and Surface Velocity (Iteration 13) at Day 9

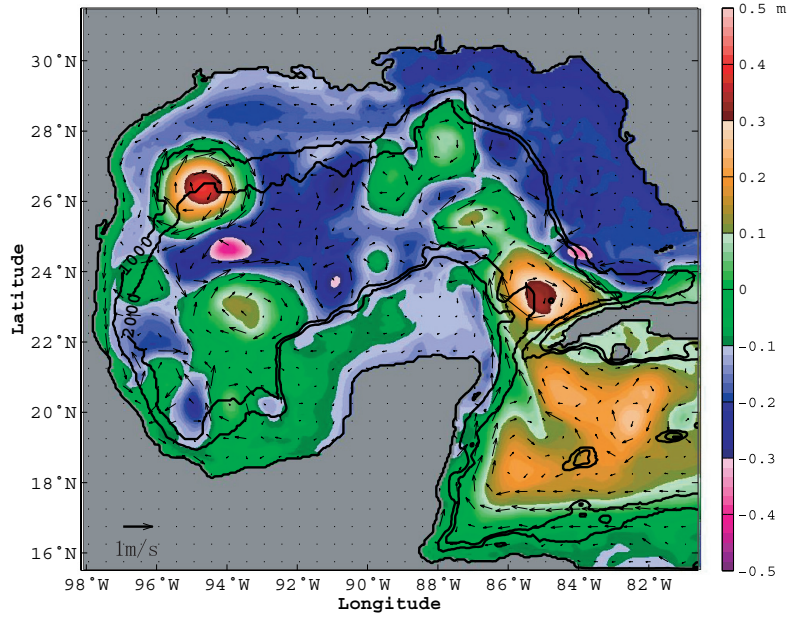


Figure 3.9. (b) The SSH and surface velocity field synoptic maps at model day 0 (top) and model day 9 (bottom) of iteration 13.

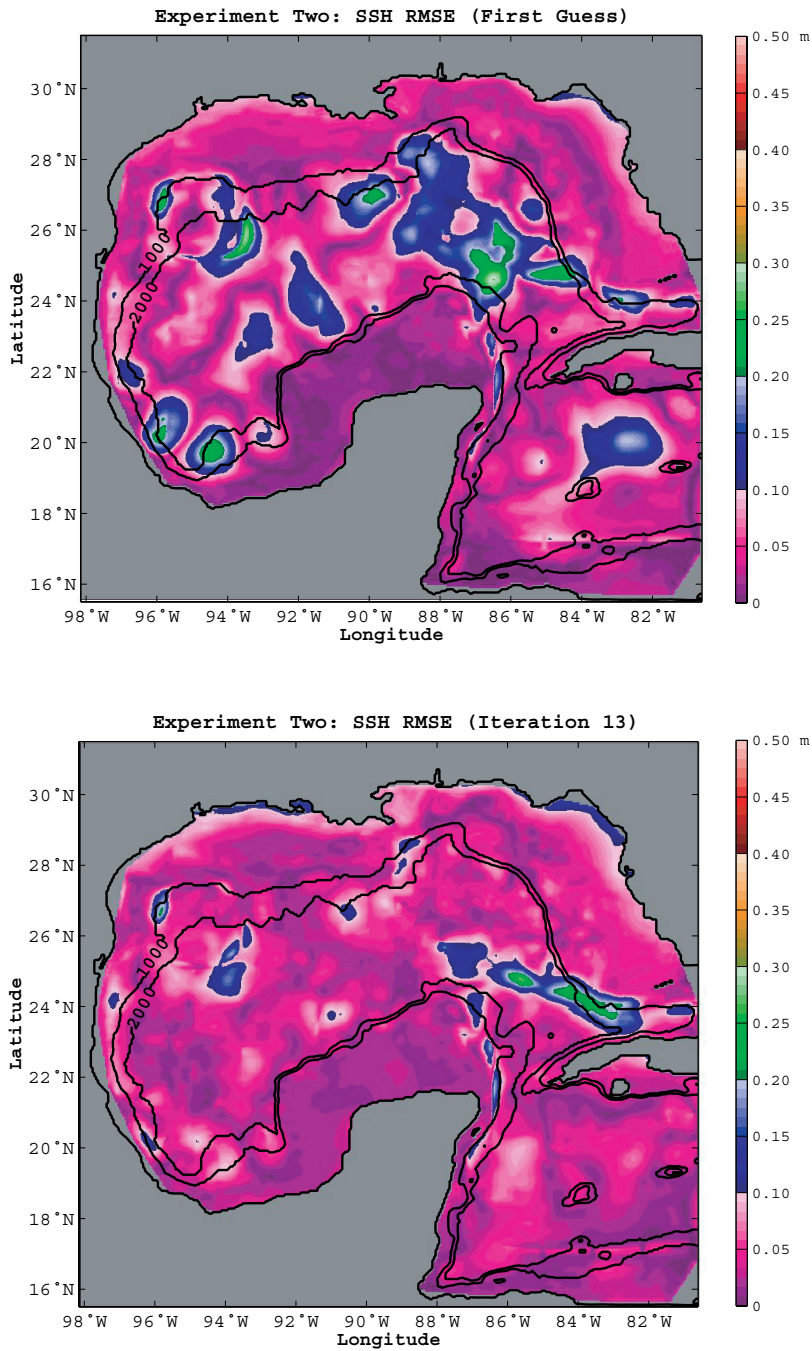


Figure 3.10. The RMSE of SSH of the initial guess (top) and iteration 13 (bottom) computed from the control run SSH fields.

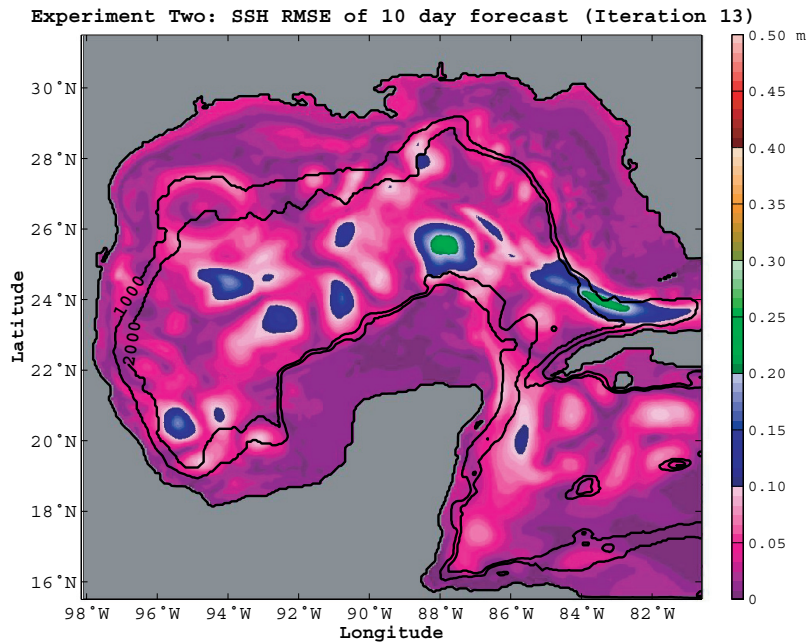
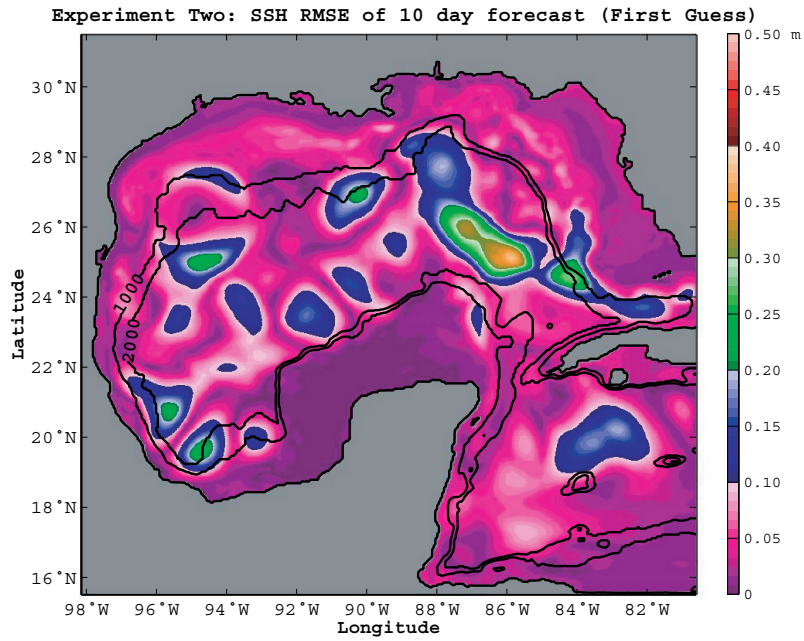


Figure 3.11. The RMSE of SSH following a 10-day forecast from the first guess (top) and from iteration 13 (bottom).

experiments from the truth field shows the improvement of the forecast achieved by improving the forecast initial state using the assimilation procedure.

3.3 Experiment Three: Application to Real Data

The data assimilation technique is applied to a real-world case in this experiment. The model configuration and the initial guess remain the same as in the previous experiments. The observation fields are derived from T/P and Jason-1 along-track SSH data and the mapping method is used to interpolate the along-track data to a regular grid. While it is acceptable for this application to assume that the observation time for each point within each ground track in the domain is the same for each cycle, the observations from different ground tracks are by no means simultaneous. Therefore, synchronization of the data from different tracks is necessary. The data from each track are processed first and interpolated to the same time grid with the mapping method, and then the same technique is applied to the synchronized data from all tracks as a whole data set to map the data to the model grid at one-day time intervals (Figure 3.12) as the observation fields to be assimilated.

The cost function decreases to 25% of its value of the first iteration at iteration ten (Figure 3.13). Visual comparison between the observations and the model outputs (Figure 3.14) and the RMSE of the model SSH relative to the gridded altimeter data (Figure 3.15) show the improvement of the SSH field by assimilating the observations. The strong anticyclonic eddy in the northwestern Gulf of Mexico, which is in the first guess but not observed by the satellite altimeters, completely disappears and the features around Cuba are successfully recovered. The assimilation procedure has the added benefit of dynamically smoothing irregularities in the mapped SSH into a more physically realistic field. It should be noted that for forecasting purposes, the field at the end of the assimilation cycle would be used as the initialization state for the forecast

model run. The SSH data are also compared over the along-track observation locations. The along-track SSH RMSE computed along the altimeter ground tracks (Figure 3.16) behaves in a manner consistent with that of the cost function and drops to 43% of its value from the first iteration.

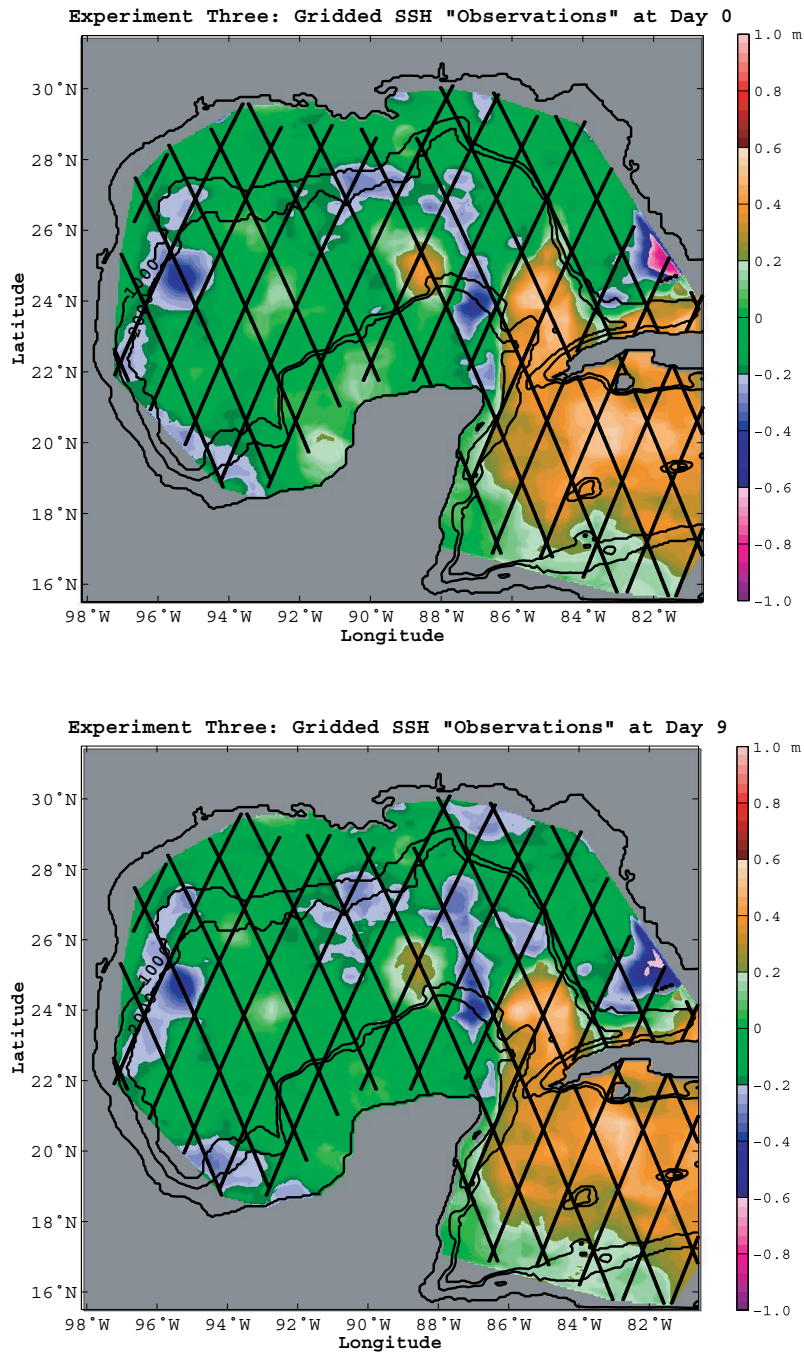


Figure 3.12. Synoptic maps of the gridded SSH fields produced using CEOF mapping method applied to T/P and Jason-1 data shown at model day 0 (January 9, 2004) and model day 9 (January 18, 2004).

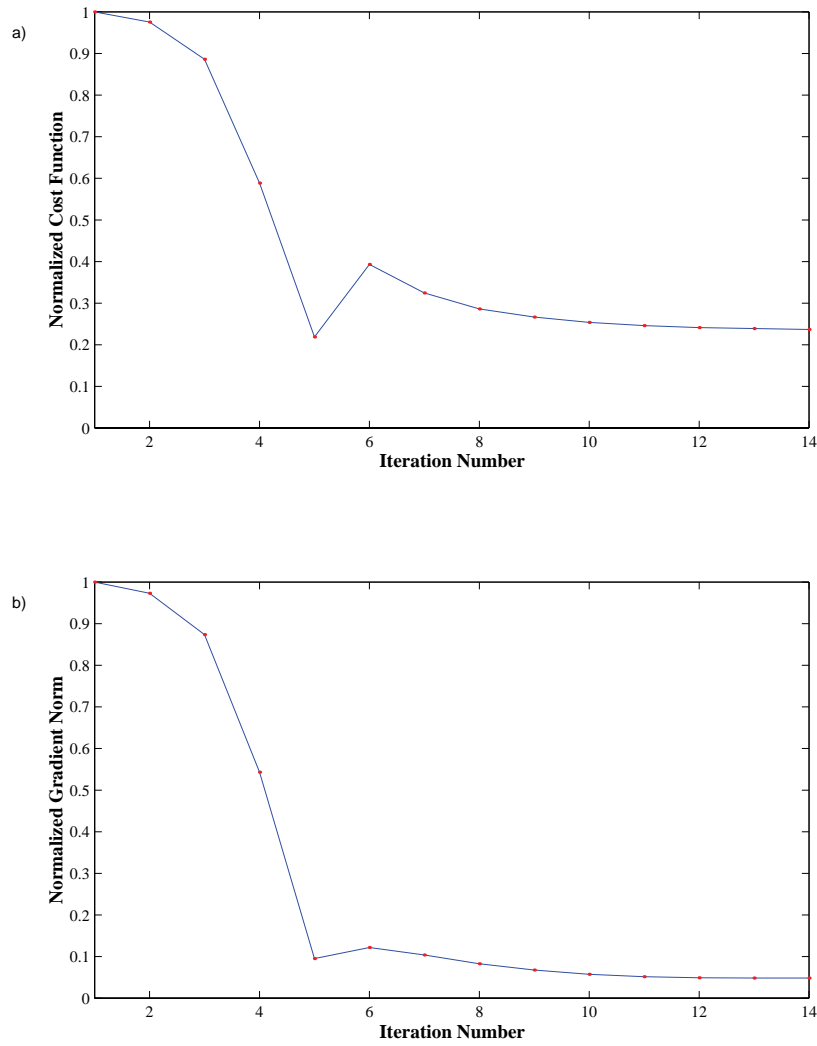
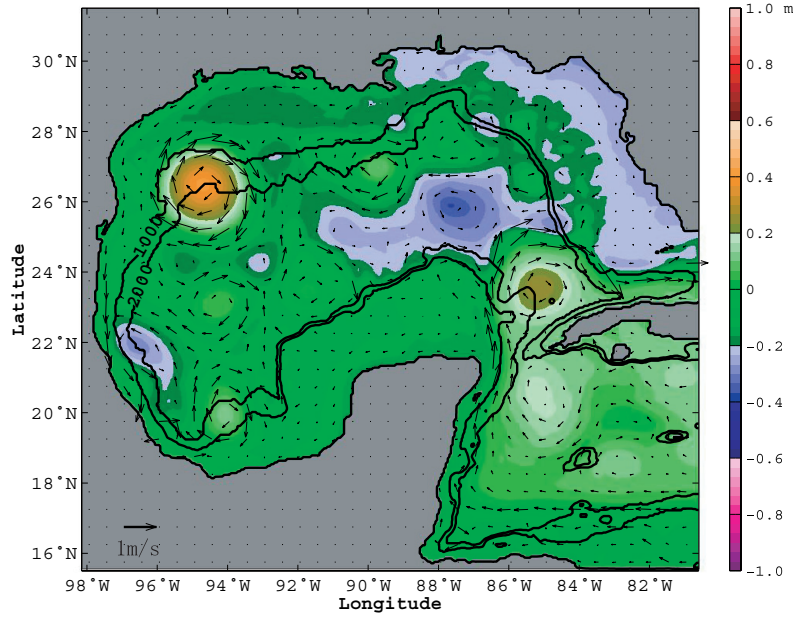


Figure 3.13. The normalized cost function (top) and the normalized gradient norm (bottom) with respect to the iteration number for experiment three.

Experiment Three: SSH and Surface Velocity (First Guess) at Day 0



Experiment Three: SSH and Surface Velocity (First Guess) at Day 9

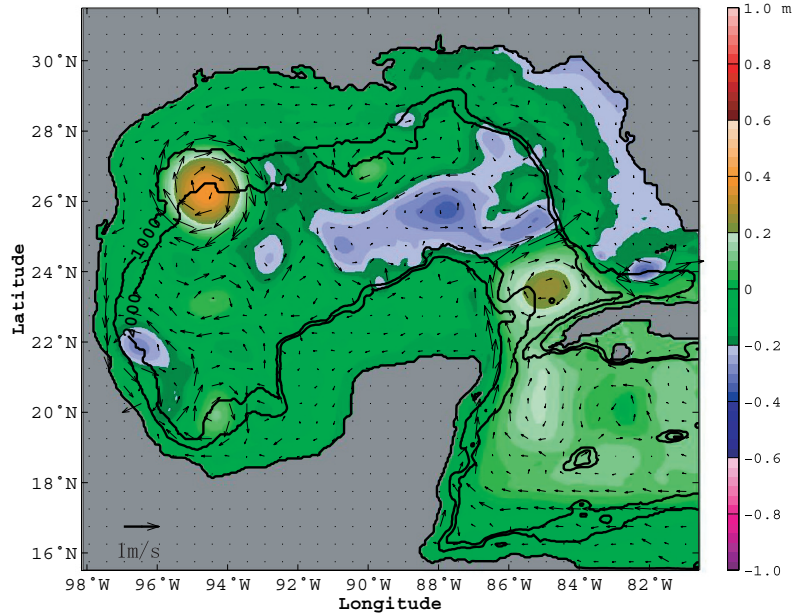
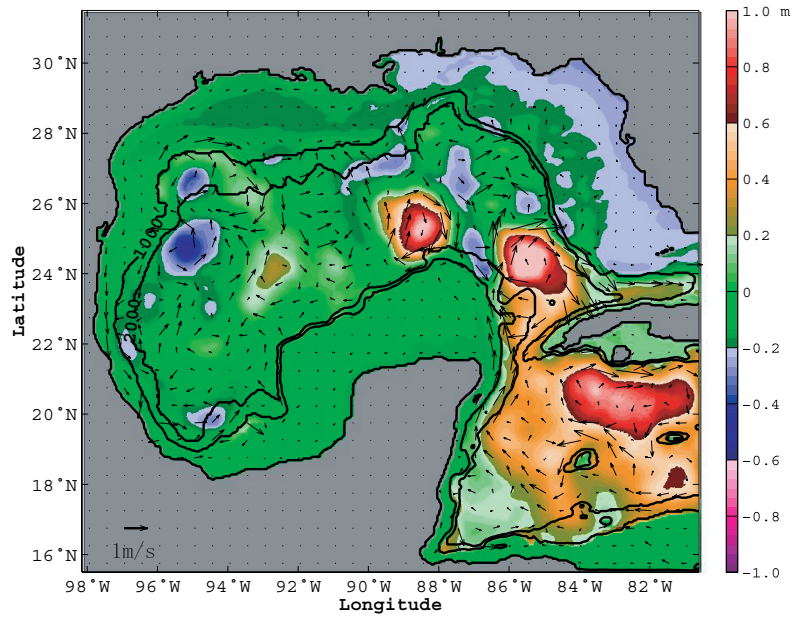


Figure 3.14. (a) Synoptic maps of SSH and surface velocity for the initial guess at model day 0 (top) and model day 9 (bottom).

Experiment Three: SSH and Surface Velocity (Iteration 14) at Day 0



Experiment Three: SSH and Surface Velocity (Iteration 14) at Day 9

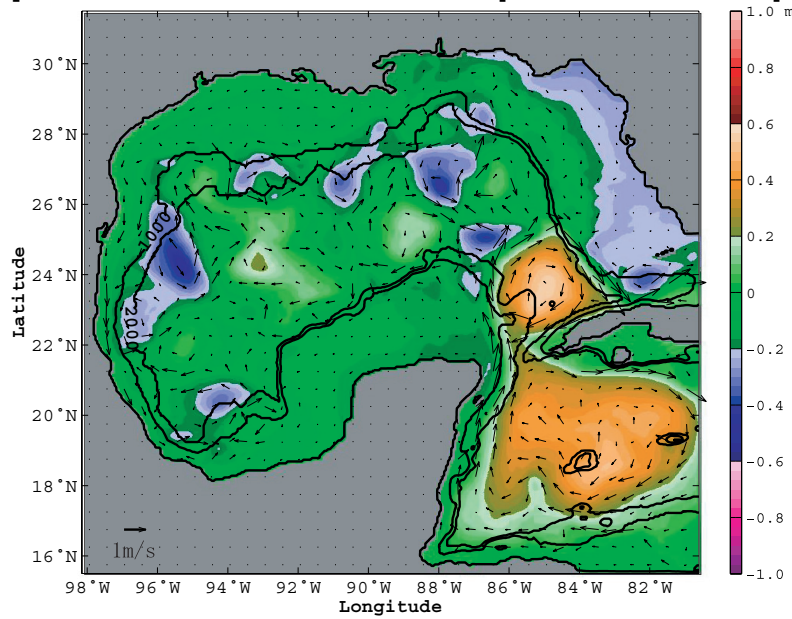


Figure 3.14. (b) Synoptic maps of SSH and surface velocity during iteration 14 at model day 0 (top) and model day 9 (bottom).

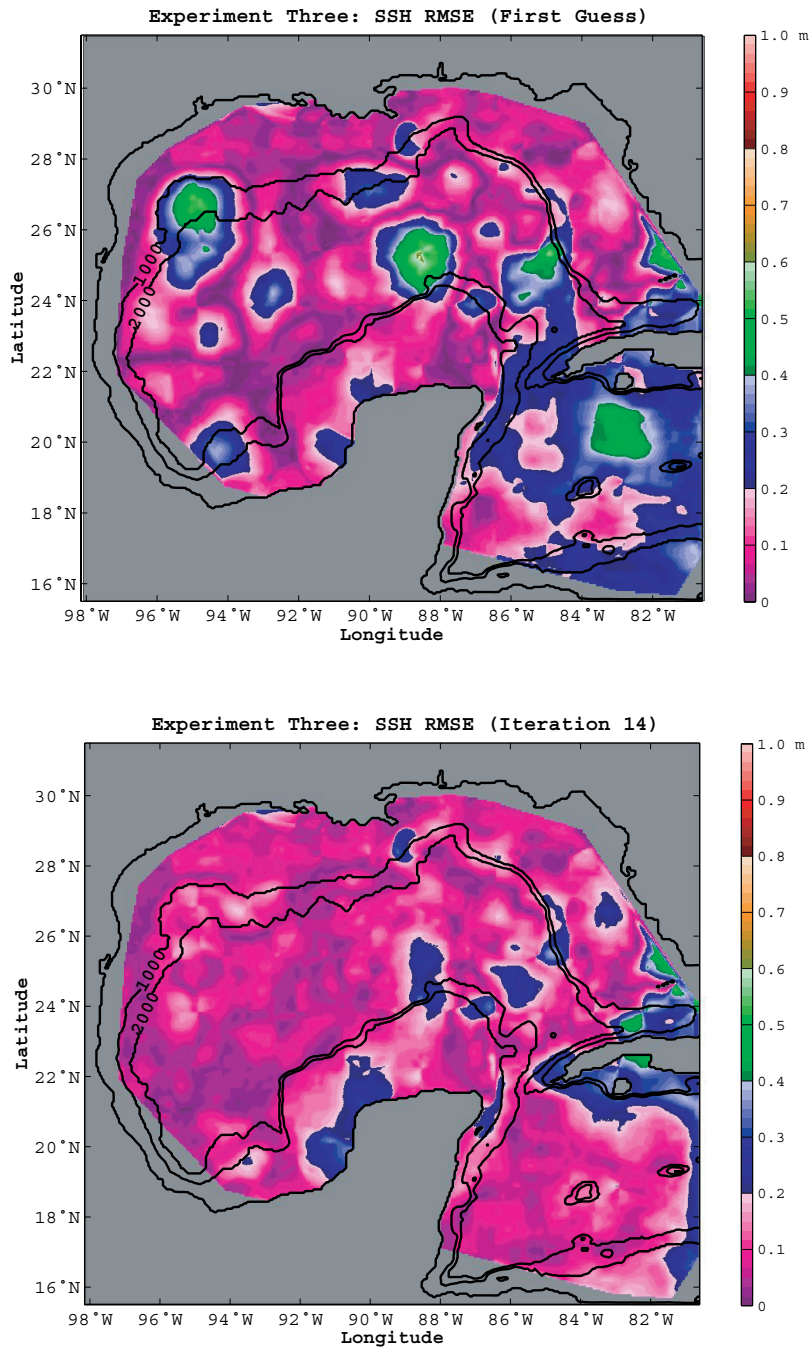


Figure 3.15. The RMSE of SSH of the initial guess (top) and iteration 14 (bottom) computed with respect to the gridded observation fields.

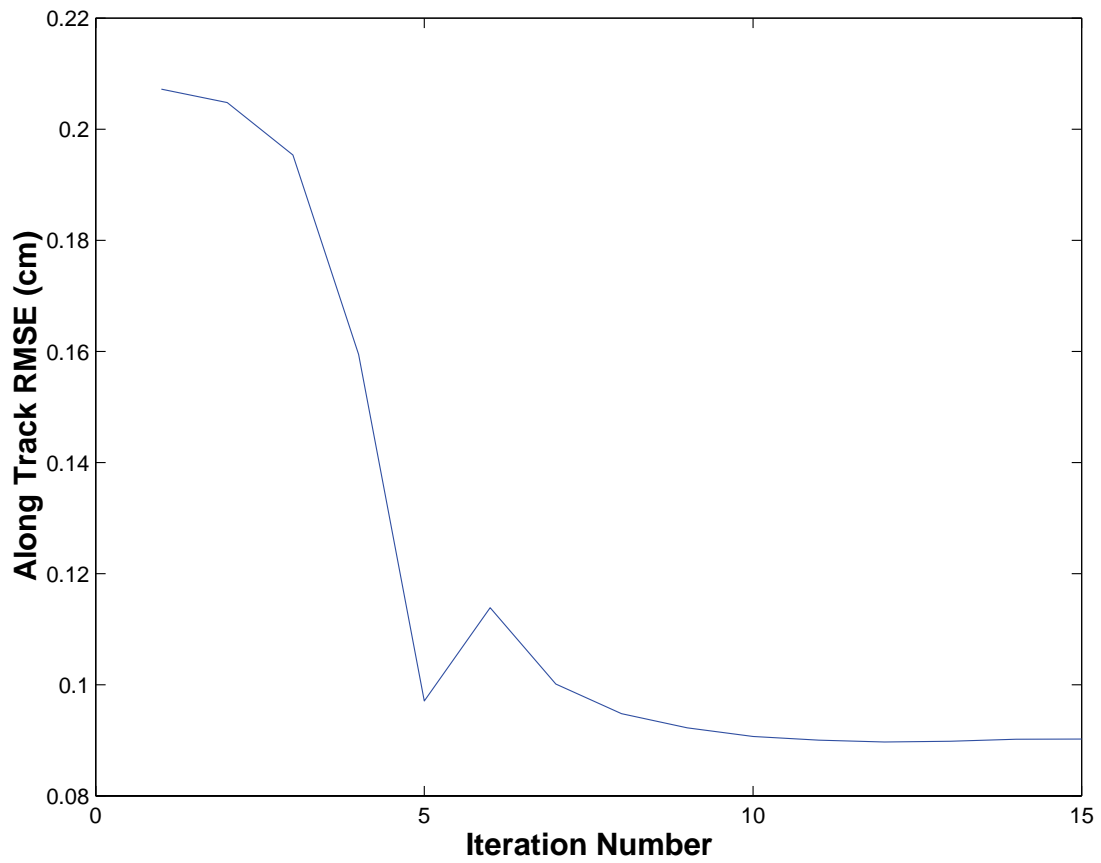


Figure 3.16. SSH RMSE between the model and the along-track satellite altimeter data plotted against iteration number.

4. DISCUSSION

The new variational data assimilation technique features several traits that may be attractive to the ocean modeling and forecasting community. This method is based on the first baroclinic mode approximation, which relies on the fact that the vertical structure of the ocean can be decomposed into different vertical normal modes. Since over much of the ocean the first baroclinic mode is dominant, it can provide a good approximation for many oceanic features of interest. This is valid especially for observations like SSH, for which the first baroclinic mode is mainly responsible. While in most conventional adjoint methods the adjoint model is constructed based on the forward model, for this research, it is constructed from an adjoint of a reduced gravity model with simplified dynamics. The forward and backward models are dynamically linked by vertical normal mode decomposition and reconstruction. As a consequence, the assimilation method is able to be designed in a modular fashion. Therefore, it could be applied to other three-dimensional ocean models without major changes as long as the first baroclinic mode is dominant in the region being modeled. This feature of the assimilation system is advantageous considering the extreme effort required for developing the adjoint of a complex ocean model. Additionally, this feature aids model intercomparison studies since different models can be run with the identical data assimilation system.

Another advantage of this data assimilation method is its potential for significantly decreasing the computational cost of applying a variational approach. Since it is based on a simplified dynamical model, the backward model requires fewer dynamical variables and is only two-dimensional (no vertical dependence) compared to the forward model with three spatial dimensions and more complicated physics. For the application

to the NCOM simulation used here, the dimension is reduced from 60 vertical layers and five prognostic variables in the forward model (and a traditional adjoint model would have the same grid size) to one vertical layer and three variables in the backward reduced gravity adjoint. Thus the backward model has a significantly lower computational cost than would an adjoint based on the forward model.

For the application of the reduced space variational method presented here, a new technique has been developed for producing regularly gridded SSH data sets from rather sparsely sampled satellite SSH observations. Poor coverage of oceanic observations requires that numerical ocean circulation models act as dynamical interpolators or extrapolators, which propagate information from data-dense areas to data-sparse regions. Since many oceanic features move quite slowly, a long assimilation cycle is required in order to provide enough time for the information transference. An alternative to this approach is the use of a statistical interpolator for the observations based on complex EOF analysis. This technique considers the propagation of information based on the observations from a much longer period compared to the assimilation window and obtains a data set with a finer regular grid. This reduces the duration of the assimilation window required for the model to capture the propagation of observed features. The preliminary results of this method indicate that it is a powerful and efficient tool for interpolating satellite along-track data. There are other good gridded SSH data sets and mapping methods that could be used in this assimilation system. However, the performance of the system crucially relies on the quality of the gridded data set and so special attention must be paid when choosing from them.

In addition to the choice of gridded SSH product for assimilation, several other choices and assumptions have been made when applying the technique for this project, and the consequences of these choices on the effectiveness of the assimilation technique must be considered. Vertical normal mode decomposition decomposes the ocean vertical structure into different vertical normal modes by separating the vertical

dependence from each mode. Vertical normal mode reconstruction uses the vertical dependence function (the eigenfunction) corresponding to the first baroclinic mode to update the first baroclinic component prior to reconstruction of the full model SSH, velocity, and density variables at the end of each assimilation iteration. This allows the assimilation system to effectively transfer information observed at the ocean surface throughout the water column in the model. Since vertical normal mode decomposition is based on the domain averaged vertical density profile in this research, a flat ocean bottom assumption is necessary. An alternative approach is to decompose the vertical structure based on the local density profile. However, experiments with this method showed that density inversions (which are highly unlikely in the mean profile) can lead to non-physical values of the equivalent depth. Further study of this issue may improve the implementation of the reduced-space variational data assimilation technique.

The conversion from the updated density fields to the temperature and salinity fields is based on their regressed relationship computed from the local profiles of these three variables. Extrapolation, which can potentially lead to errors in the updated temperature and salinity fields, is sometimes necessary when using this algorithm, so quality control checks must be performed. Other methods of mapping the updated density fields onto the model temperature and salinity fields could be developed and incorporated into the assimilation system in order to improve its performance.

In the data assimilation technique, the purpose of running a backward model is to compute the gradient of the cost function with respect to the model control variables. Since the backward model in this research is based on the reduced gravity model approximating the first baroclinic mode, traditionally the cost function would have been defined in a consistent way based on the first baroclinic mode component. However, since the only observation assumed to be available is the SSH, vertical normal mode decomposition cannot be applied to get the first baroclinic mode component of the SSH without observing the ocean's vertical structure. Thus, the cost function is defined using

the full SSH field (that is, the distance between the full model SSH and the SSH observational field). Though this is a reasonable approximation considering the dominance of the first baroclinic mode in the SSH field, this and other assumptions made during the application of the assimilation method lead to some unusual behavior of the cost function compared to other studies using the variational data assimilation method. For example, the cost function is not always a monotonically decreasing function and does not always converge to a small value.

5. SUMMARY

A new variational data assimilation technique based on the first baroclinic mode approximation of the three-dimensional ocean dynamics has been developed and tested in this study. The results of the tests conducted with this technique demonstrate that it is a viable alternative to the conventional variational data assimilation method for assimilating satellite altimeter data into a three-dimensional ocean model. The modular design makes the assimilation system more flexible; not only the ocean model, but also the other components of the system can be replaced with different techniques and algorithms. For example, a different statistical interpolation algorithm, or mapping from density to temperature and salinity could be substituted rather easily. The incorporation of the statistical interpolator and vertical normal mode decomposition contributes to a more computationally efficient data assimilation system. The mapping technique successfully recovers the information in data-sparse areas (areas between satellite altimeter ground tracks in this study) and makes the assimilation window shorter. The computational cost is also reduced by using an adjoint based on a one-active-layer reduced gravity model with simplified dynamics, which leads to a reduced number of dimensions and model variables in the backward model.

Forecasting mesoscale ocean processes requires accurate initial conditions that can be improved by assimilating observational data. The application of the new data assimilation technique for initializing an ocean forecast is summarized as follows. First, the ocean dynamics within a model region must be analyzed to ensure that the assumption that the SSH is dominated by the first baroclinic mode is valid. Next, the forward model is integrated for some assimilation time period. A cost function is

computed, which involves the forward model SSH misfit to a prescribed SSH observational field (in the test cases, a new CEOF based interpolation method has been used to construct this SSH field from satellite altimeter data). The three-dimensional model fields are decomposed into their vertical normal modes, and the first baroclinic mode variables are used in computing the reduced gravity adjoint model, which is integrated backward in time. The gradient of the cost function with respect to the model control variables is used to adjust the variables to reduce the size of the cost function based on a numerical optimization method (the L-BFGS method). The adjusted first baroclinic mode variables are then substituted to reconstruct the full model fields at the beginning of the forward model integration time by summing their vertical modes. This procedure is iterated initializing the forward model with the updated fields until the cost function asymptotes to some small value. As a consequence of simplifications and assumptions made to the variational data assimilation method, a perfect convergence of the cost function may not be obtained. Finally, the model fields at the end of the forward model integration at the last iteration provide a more accurate description of the state of the ocean at that time than the first guess, and can be used to initialize an ocean model forecast.

The main goal of this study is to develop a new effective and efficient method for assimilating satellite altimeter data that can be applied to a number of different ocean models. The method has been successfully applied to a model of the Gulf of Mexico that has high resolution in all three spatial dimensions. Experiments have been conducted to test the effectiveness of the method, and to demonstrate its applicability to a real-world case by assimilating an SSH data set produced from satellite altimeter data using a new gridding technique. It is not assumed that all the choices made for these tests will ultimately prove to be the best. Nevertheless, the technique shows great promise for future studies and possibly operational implementation. The quality and performance of the assimilation system can likely be improved by replacing some algorithms used in the application of this research with other options, which shows the

advantage of the modularly designed system.

APPENDIX A

VERTICAL NORMAL MODE DECOMPOSITION FROM NCOM EQUATIONS

Following Philander (1990), a method of computing vertical normal modes is derived from the NCOM model equations. The NCOM equations are as given in continuous form in equations (2.28-2.34). The model equations are simplified as follows.

First, the equation of state is simplified to a linear form as

$$\rho = \rho_0[1 - \alpha(T - T_0) + \beta(S - S_0)] \quad (1A)$$

where $\alpha = -\frac{1}{\rho_0} \frac{\partial \rho}{\partial T}$, and $\beta = \frac{1}{\rho_0} \frac{\partial \rho}{\partial S}$.

So the time dependence of density can be written as

$$\frac{d\rho}{dt} = \frac{\partial \rho}{\partial T} \Big|_s \frac{dT}{dt} + \frac{\partial \rho}{\partial S} \Big|_T \frac{dS}{dt} = -\alpha \rho_0 \frac{dT}{dt} + \beta \rho_0 \frac{dS}{dt}. \quad (2A)$$

Expanding the material time derivative as

$$\frac{1}{\rho_0} \left(\frac{\partial \rho}{\partial t} + \nabla \cdot (\mathbf{v}\rho) \right) = -\alpha \left(\frac{\partial T}{\partial t} + \nabla \cdot (\mathbf{v}T) \right) + \beta \left(\frac{\partial S}{\partial t} + \nabla \cdot (\mathbf{v}S) \right) \quad (3A)$$

allows the equations (2.32) and (2.33) to be substituted to obtain the form

$$\frac{1}{\rho_0} \left(\frac{\partial \rho}{\partial t} + \nabla \cdot (\mathbf{v}\rho) \right) = -\alpha [QT + \nabla_h (A_H \nabla_h T) + (K_H T_z)_z + Q_r \gamma_z] + \beta [QS + \nabla_h (A_H \nabla_h S) + (K_H S_z)_z] \quad (4A)$$

where the subscript z stands for $\partial/\partial z$ and the subscript t stands for $\partial/\partial t$.

By again using equation (1A) it can be shown that

$$\rho_0^{-1} \nabla_h (A_H \nabla_h \rho) = -\alpha \nabla_h (A_H \nabla_h T) + \beta \nabla_h (A_H \nabla_h S), \quad (5A)$$

and

$$\rho_0^{-1} (K_H \rho_z)_z = -\alpha (K_H T_z)_z + \beta (K_H S_z)_z. \quad (6A)$$

Substituting (5A) and (6A) into (4A) gives a prognostic equation for density

$$\rho_t / \rho_0 = -\rho_0^{-1} \nabla \cdot (\mathbf{v}\rho) + Q(-\alpha T + \beta S) + \rho_0^{-1} \nabla_h (A_H \nabla_h \rho) + \rho_0^{-1} (K_H \rho_z)_z - \alpha Q_r \gamma_z \quad (7A)$$

that can replace equations (2.32-2.34). Equation (7A) and equations (2.28-2.31) are the reduced set of equations.

The problem needs to be further simplified by linearization of the above equations. To linearize these equations it is necessary to assume that the ocean, in its basic state, is

motionless and has density $\rho = \bar{\rho}(z)$, which is a function of depth only. Motion and its associated density variation $\rho'(x, y, z, t)$ are considered as small perturbations to this basic state. For the sake of mathematical convenience, it is assumed that $K_M = K_H = A/N^2$, where N is defined as $N = (-g\bar{\rho}_z/\rho_0)^{1/2}$ (the Brunt-Väisälä frequency) and A is a constant.

With these assumptions and neglecting the source term Q and solar radiation Q_r , the linearized unforced NCOM equations become

$$\frac{\partial u}{\partial t} = fv - \frac{1}{\rho_0} \frac{\partial p}{\partial x} + \frac{\partial}{\partial z} \left(\frac{A}{N^2} \frac{\partial u}{\partial z} \right), \quad (8A)$$

$$\frac{\partial v}{\partial t} = -fu - \frac{1}{\rho_0} \frac{\partial p}{\partial y} + \frac{\partial}{\partial z} \left(\frac{A}{N^2} \frac{\partial v}{\partial z} \right), \quad (9A)$$

$$\frac{\partial p}{\partial z} = -\rho g, \quad (10A)$$

$$\frac{\partial u}{\partial x} + \frac{\partial v}{\partial y} + \frac{\partial w}{\partial z} = 0, \quad (11A)$$

$$\frac{\partial \rho}{\partial t} = -\nabla \cdot (\mathbf{v}\rho) + \nabla_h (A_H \nabla_h \rho) + \frac{\partial}{\partial z} \left(\frac{A}{N^2} \frac{\partial \rho}{\partial z} \right) \approx -w \frac{\partial \rho}{\partial z} + \frac{\partial}{\partial z} \left(\frac{A}{N^2} \frac{\partial \rho}{\partial z} \right), \text{ i.e.,}$$

$$\frac{\partial \rho}{\partial t} = \rho_0 w \frac{N^2}{g} + \frac{\partial}{\partial z} \left(\frac{A}{N^2} \frac{\partial \rho}{\partial z} \right). \quad (12A)$$

ρ is eliminated by substituting (10A) into (12A) yielding

$$p_{zt} + \rho_0 w N^2 = \frac{\partial}{\partial z} \left(\frac{A}{N^2} p_{zz} \right). \quad (13A)$$

The method of separation of variables is applied by assuming

$$u = \sum_{m=0}^M U_m(x, y, t) R_m(z), \quad (14A)$$

$$v = \sum_{m=0}^M V_m(x, y, t) R_m(z), \quad (15A)$$

$$\frac{p}{g\rho_0} = \sum_{m=0}^M \eta_m(x, y, t) R_m(z), \quad (16A)$$

$$w = \sum_{m=0}^M W_m(x, y, t) S_m(z), \quad (17A)$$

where m is the mode number and M is the upper limit for m which goes to infinity for continuous functions.

Substitution yields

$$(U_t - fV + g\eta_x)R = \left(\frac{A}{N^2}UR_z\right)_z, \quad (18A)$$

$$(V_t + fU + g\eta_y)R = \left(\frac{A}{N^2}VR_z\right)_z, \quad (19A)$$

$$(U_x + V_y)R + WS_z = 0, \quad (20A)$$

$$\eta_t R_z + \frac{WN^2}{g}S = \left(\frac{A}{N^2}\eta R_{zz}\right)_z, \quad (21A)$$

where the subscript m has been dropped. By rewriting (20A) as

$$\frac{U_x + V_y}{-W} = \frac{S_z}{R} = -\frac{1}{gh}, \quad (22A)$$

where h is the constant of separation, one gets

$$R = -ghS_z. \quad (23A)$$

Separating the z-dependence in (18A) and (19A) yields

$$\frac{U_t - fV + g\eta_x}{AU} = \frac{(R_z/N^2)_z}{R} = -\frac{1}{gh}, \quad (24A)$$

and

$$\frac{V_t + fU + g\eta_y}{AV} = \frac{(R_z/N^2)_z}{R} = -\frac{1}{gh}. \quad (25A)$$

Both (24A) and (25A) lead to

$$\left(\frac{R_z}{N^2}\right)_z = -\frac{R}{gh}. \quad (26A)$$

Plugging (23A) into (26A) yields

$$S_z + gh\left(\frac{S_{zz}}{N^2}\right)_z = 0 \quad (27A)$$

which is integrated vertically to arrive at the relation

$$S + gh\frac{S_{zz}}{N^2} = C \quad (28A)$$

where C is an arbitrary constant.

Assuming $S = 0$ and $S_{zz} = 0$ at the bottom leads to $C = 0$ and (28A) turns to

$$\frac{S_{zz}}{N^2} + \frac{S}{gh} = 0. \quad (29A)$$

The boundary conditions are given by

$$w = S = 0 \quad z = z_{bottom}, \quad (30A)$$

$$w - \frac{p_t}{\rho_0 g} = 0, \quad z = 0. \quad (31A)$$

Substituting (16A) and (17A) into (31A) leads to

$$WS - \eta_t = 0, \text{ i.e.,}$$

$$WS - \eta_t \frac{-WS_z}{U_x + V_y} = 0.$$

So,

$$S - hS_z = 0. \quad (32A)$$

Thus, the vertical normal mode decomposition problem is reduced to the following equations:

$$U_t - fV + g\eta_x = -AU/gh, \quad (33A)$$

$$V_t + fU + g\eta_y = -AV/gh, \quad (34A)$$

$$\eta_t + h(U_x + V_y) = -A\eta/gh, \quad (35A)$$

$$S_{zz} + \frac{N^2}{gh}S = 0, \quad (36A)$$

$$R = -ghS_z \quad (37A)$$

with boundary conditions:

$$S_t = 0, \quad z = z_{bottom}, \quad (38A)$$

$$S - hS_z = 0, \quad z = 0. \quad (39A)$$

(36A) along with the boundary conditions (38A) and (39A) is a Sturm-Liouville problem, and the discrete version is an eigenvalue problem, which can be solved via standard numerical methods. (33A), (34A) and (35A) are governing equations for each mode, which are shallow-water equations.

From (36A) and (37A), the equation for R is

$$\left(\frac{R_z}{N^2}\right)_z + \frac{R}{gh} = 0. \quad (40A)$$

Based on the Sturm-Liouville general solution, the eigenfunctions, R_n , form a complete set and are orthogonal in the sense that

$$\int_{-H}^0 R_m R_n dz = 0 \quad m \neq n. \quad (41A)$$

The baroclinic modes can be obtained as

$$\int_{-H}^0 u R_n dz = \int_{-H}^0 \left[\sum_m U_m R_m \right] R_n dz = \sum_m U_m \int_{-H}^0 R_m R_n dz = U_n \int_{-H}^0 R_n^2 dz. \quad (42A)$$

So,

$$U_n = \int_{-H}^0 u R_n dz \Big/ \int_{-H}^0 R_n^2 dz. \quad (43A)$$

Similarly,

$$V_n = \int_{-H}^0 v R_n dz \Big/ \int_{-H}^0 R_n^2 dz, \quad (44A)$$

$$\eta_n = \int_{-H}^0 \frac{p}{g\rho_0} R_n dz \Big/ \int_{-H}^0 R_n^2 dz. \quad (45A)$$

APPENDIX B

DERIVATION OF THE ADJOINT OF THE REDUCED GRAVITY MODEL

Adjoint equations are derived from the equations for a reduced gravity ocean model, using the calculus of variations and forming a Lagrange cost function by adding the constraints multiplied by the Lagrange multipliers.

The cost function is defined as

$$F = K_m \int (\eta(x, y, t) - \eta_{obs}(x, y, t))^2 dx dy dt + \int \left[\frac{\lambda_u}{\alpha} \cdot (33A) + \frac{\lambda_v}{\alpha} \cdot (34A) + \lambda_\eta \cdot (35A) \right] dx dy dt. \quad (1B)$$

Assuming the observation errors at different locations are uncorrelated and the observation error variances are constant reduces K_m to a constant. So (1B) can be rewritten as

$$F = \frac{1}{\alpha} \int_{x,y,t} \lambda_u [U_t - fV + g\eta_x + AU/gh] dx dy dt \quad (I)$$

$$+ \frac{1}{\alpha} \int_{x,y,t} \lambda_v [V_t + fU + g\eta_y + AV/gh] dx dy dt \quad (II)$$

$$+ \int_{x,y,t} \lambda_h [\eta_t + h(U_x + V_y) + A\eta/gh] dx dy dt \quad (III)$$

$$+ K_m \int (\eta(x, y, t) - \eta_{obs}(x, y, t))^2 dx dy dt \quad (IV) \quad (2B)$$

where λ_u , λ_v , and λ_h are the adjoint variables with respect to the control variables, U , V , and η . At the minimum of the cost function, F has a stationary point, and its first variation with respect to all control variables must vanish. In order to find the adjoint equations, one has to set the first derivative of the associated Lagrange function to zero, *i.e.*,

$$\frac{\partial F}{\partial U} = 0, \quad (3B)$$

$$\frac{\partial F}{\partial V} = 0, \quad (4B)$$

and

$$\frac{\partial F}{\partial \eta} = 0. \quad (5B)$$

(3B) is considered first:

$$\begin{aligned} \frac{\partial}{\partial U} \frac{1}{\alpha} \int_{x,y,t} \lambda_u [U_t] dx dy dt &= \frac{1}{\alpha} \frac{\partial}{\partial U} \left[\int_{x,y,t} \frac{\partial}{\partial t} (\lambda_u U) dx dy dt - \int_{x,y,t} U \frac{\partial \lambda_u}{\partial t} dx dy dt \right] \\ &= -\frac{1}{\alpha} \int_{x,y,t} \frac{\partial \lambda_u}{\partial t} dx dy dt \end{aligned} \quad (6B)$$

where the initial conditions, $\lambda_u|_{t=\tau} = 0$ and $U|_{t=0}$ are used.

$$\frac{\partial}{\partial U} \frac{1}{\alpha} \int_{x,y,t} \lambda_u \left[\frac{AU}{gh} \right] dx dy dt = \frac{1}{\alpha} \int_{x,y,t} \frac{A\lambda_u}{gh} dx dy dt, \quad (7B)$$

$$\frac{\partial}{\partial U} \frac{1}{\alpha} \int_{x,y,t} \lambda_v [fU] dx dy dt = \frac{1}{\alpha} \int_{x,y,t} f \lambda_v dx dy dt, \quad (8B)$$

$$\begin{aligned} \frac{\partial}{\partial U} \int_{x,y,t} \lambda_h [hU_x] dx dy dt &= \frac{\partial}{\partial U} \left[h \int_{x,y,t} (\lambda_h U)_x dx dy dt - h \int_{x,y,t} U \frac{\partial \lambda_h}{\partial x} dx dy dt \right] \\ &= - \int_{x,y,t} h \frac{\partial \lambda_h}{\partial x} dx dy dt. \end{aligned} \quad (9B)$$

So, the governing equation for λ_u is

$$\frac{1}{\alpha} \frac{\partial \lambda_u}{\partial t} - \frac{1}{\alpha} f \lambda_v + h \frac{\partial \lambda_h}{\partial x} = \frac{1}{\alpha} \frac{A \lambda_u}{gh}. \quad (10B)$$

Similarly, when (4B) is considered,

$$\frac{\partial}{\partial V} \frac{1}{\alpha} \int_{x,y,t} \lambda_u [-fV] dx dy dt = -\frac{1}{\alpha} \int_{x,y,t} f \lambda_u dx dy dt, \quad (11B)$$

$$\begin{aligned} \frac{\partial}{\partial V} \frac{1}{\alpha} \int_{x,y,t} \lambda_v [V_t] dx dy dt &= \frac{1}{\alpha} \frac{\partial}{\partial V} \left[\int_{x,y,t} \frac{\partial}{\partial t} (\lambda_v V) dx dy dt - \int_{x,y,t} V \frac{\partial \lambda_v}{\partial t} dx dy dt \right] \\ &= -\frac{1}{\alpha} \int_{x,y,t} \frac{\partial \lambda_v}{\partial t} dx dy dt, \end{aligned} \quad (12B)$$

$$\frac{\partial}{\partial V} \frac{1}{\alpha} \int_{x,y,t} \lambda_v \left[\frac{AV}{gh} \right] dx dy dt = \frac{1}{\alpha} \int_{x,y,t} \frac{A \lambda_v}{gh} dx dy dt, \quad (13B)$$

$$\begin{aligned} \frac{\partial}{\partial V} \int_{x,y,t} \lambda_h [hV_y] dx dy dt &= \frac{\partial}{\partial V} \left[h \int_{x,y,t} (\lambda_h V)_y dx dy dt - h \int_{x,y,t} V \frac{\partial \lambda_h}{\partial y} dx dy dt \right] \\ &= - \int_{x,y,t} h \frac{\partial \lambda_h}{\partial y} dx dy dt. \end{aligned} \quad (14B)$$

So, the governing equation for λ_v is

$$\frac{1}{\alpha} \frac{\partial \lambda_v}{\partial t} + \frac{1}{\alpha} f \lambda_u + h \frac{\partial \lambda_v}{\partial y} = \frac{1}{\alpha} \frac{A \lambda_v}{gh}. \quad (15B)$$

Consider (5B),

$$\begin{aligned} \frac{\partial}{\partial \eta} \frac{1}{\alpha} \int_{x,y,t} \lambda_u [g \eta_x] dx dy dt &= \frac{1}{\alpha} \frac{\partial}{\partial \eta} \left[\int_{x,y,t} g \frac{\partial}{\partial x} (\lambda_u \eta) dx dy dt - \int_{x,y,t} g \eta \frac{\partial \lambda_u}{\partial x} dx dy dt \right] \\ &= -\frac{1}{\alpha} \int_{x,y,t} g \frac{\partial \lambda_u}{\partial x} dx dy dt. \end{aligned} \quad (16B)$$

Similarly,

$$\begin{aligned} \frac{\partial}{\partial \eta} \frac{1}{\alpha} \int_{x,y,t} \lambda_v [g \eta_y] dx dy dt &= \frac{1}{\alpha} \frac{\partial}{\partial \eta} \left[\int_{x,y,t} g \frac{\partial}{\partial y} (\lambda_v \eta) dx dy dt - \int_{x,y,t} g \eta \frac{\partial \lambda_v}{\partial y} dx dy dt \right] \\ &= -\frac{1}{\alpha} \int_{x,y,t} g \frac{\partial \lambda_v}{\partial y} dx dy dt, \end{aligned} \quad (17B)$$

$$\begin{aligned} \frac{\partial}{\partial \eta} \int_{x,y,t} \lambda_h [\eta_t] dx dy dt &= \frac{\partial}{\partial \eta} \left[\int_{x,y,t} (\lambda_h \eta)_t dx dy dt - \int_{x,y,t} \eta \frac{\partial \lambda_h}{\partial t} dx dy dt \right] \\ &= -\int_{x,y,t} \frac{\partial \lambda_h}{\partial t} dx dy dt, \end{aligned} \quad (18B)$$

$$\frac{\partial}{\partial \eta} \int_{x,y,t} \lambda_h \left[\frac{A \eta}{gh} \right] dx dy dt = \int_{x,y,t} \frac{A \lambda_h}{gh} dx dy dt, \quad (19B)$$

$$\frac{\partial}{\partial \eta} K_m \int_{x,y,t} [\eta - \eta_{obs}]^2 dx dy dt = 2K_m \int_{x,y,t} (\eta - \eta_{obs}) dx dy dt. \quad (20B)$$

So, the governing equation for λ_h is

$$\frac{\partial \lambda_h}{\partial t} + \frac{g}{\alpha} \left(\frac{\partial \lambda_u}{\partial x} + \frac{\partial \lambda_v}{\partial y} \right) = \frac{A \lambda_h}{gh} + 2K_m (\eta - \eta_{obs}). \quad (21B)$$

Reorganize the above equations

$$\frac{\partial \lambda_u}{\partial t} - f \lambda_v + \alpha h \frac{\partial \lambda_h}{\partial x} = \frac{A \lambda_u}{gh}, \quad (22B)$$

$$\frac{\partial \lambda_v}{\partial t} + f \lambda_u + \alpha h \frac{\partial \lambda_h}{\partial y} = \frac{A \lambda_v}{gh}, \quad (23B)$$

$$\frac{\partial \lambda_h}{\partial t} + \frac{g}{\alpha} \left(\frac{\partial \lambda_u}{\partial x} + \frac{\partial \lambda_v}{\partial y} \right) = \frac{A \lambda_h}{gh} + 2K_m (\eta - \eta_{obs}). \quad (24B)$$

For the scaling purposes, let $\alpha = g/h$, and the equations become

$$\frac{\partial \lambda_u}{\partial t} - f \lambda_v + g \frac{\partial \lambda_h}{\partial x} = \frac{A \lambda_u}{gh}, \quad (25B)$$

$$\frac{\partial \lambda_v}{\partial t} + f \lambda_u + g \frac{\partial \lambda_h}{\partial y} = \frac{A \lambda_v}{gh}, \quad (26B)$$

$$\frac{\partial \lambda_h}{\partial t} + h \left(\frac{\partial \lambda_u}{\partial x} + \frac{\partial \lambda_v}{\partial y} \right) = \frac{A \lambda_h}{gh} + 2K_m (\eta - \eta_{obs}). \quad (27B)$$

REFERENCES

- Anderson, J. L., 2001: An ensemble adjustment Kalman Filter for data assimilation. *Mon. Wea. Rev.* **129**, 2884-2903.
- Anthes, R. A., 1974: Data assimilation and initialization of hurricane prediction models. *J. Atmos. Sci.*, **31**, 702-719.
- Barnett, T. P., 1983: Interaction of the monsoon and Pacific trade wind system at interannual time scales. Part I: The equatorial zone. *Mon. Wea. Rev.*, **111**, 756-773.
- Bergthorsson, P., and B. Doos, 1955: Numerical weather map analysis. *Tellus*, **7**, 329-340.
- Cohn, S. E., 1982: *Methods of sequential estimation for determining initial data in numerical weather prediction*. Ph.D. Thesis, New York University, 183 pp.
- Courtier, P., and O. Talagrand, 1987: Variational assimilation of meteorological observations with the adjoint vorticity equation. Part II: Numerical results. *Q. J. R. Meteorol. Soc.*, **113**, 1329-1368.
- Courtier, P., and O. Talagrand, 1990: Variational assimilation of meteorological observations with the direct and adjoint shallow-water equation. *Tellus*, **42A**, 531-549.
- Daley, R., 1991: *Atmospheric data analysis*. Cambridge University Press, Cambridge, 457 pp.
- DaSilva, A., A. C. Young, and S. Levitus, 1994: *Atlas of Surface Marine Data 1994*, vol. **1**, *Algorithms and Procedures*, NOAA Atlas NESDIS 6, Natl. Oceanic and Atmos. Admin., Silver Spring, Md..
- Deber, J. C., 1987: Variational four-dimensional analysis using quasi-geostrophic constraints. *Mon. Wea. Rev.*, **115**, 998-1008.
- Dewar, W. K., and M.Y. Morris, 2000: On the propagation of baroclinic waves in the general circulation, *J. Phys. Oceanogr.*, **30**, 2637-2649.
- Dewar, W. K., and R. X. Huang, 2001: Adjustment of the ventilated thermocline. *J.*

Phys. Oceanogr., **31**, 1676-1697.

Gilchrist, B., and G. P. Cressman, 1954: An experiment in objective analysis. *Tellus*, **6**, 309-318.

Ghil, M., S. E. Cohn, J. Tavantzis, K. Bube, and E. Isaacson, 1981: Application of estimation theory to numerical weather prediction. *Dynamical Meteorology: Data Assimilation Methods*, L. Bengtsson, M. Gill and E. Kallen, Eds., Springer-Verlag, 139-224.

Gill, M., and P. Malanotte-Rizzoli. 1991: Data assimilation in meteorology and oceanography. *Adv. Geophys.*, **33**, 141-266

Houtekamer, P. L., and H. L. Michell, 1998: Data assimilation using an ensemble Kalman filter technique. *Mon. Wea. Rev.* **126**, 796-811.

Houtekamer, P. L., and H. L. Mitchell, 2001: A sequential ensemble Kalman filter for atmospheric data assimilation. *Mon. Wea. Rev.* **129**, 123-137.

Kalman, R. E., 1960: A new approach to linear filtering and prediction problems. *Trans. ASME, J. Basic Eng.*, **82D**, 35-45.

Kalman, R. E., and R. S. Bucy, 1961: New results in linear filtering and prediction problems. *Trans. ASME, J. Basic Eng.*, **82D**, 35-45.

Kalnay, E., 2002: *Atmospheric modeling, data assimilation and predictability*. Cambridge University Press, Cambridge, 341 pp.

Le Dimet, F. X., and I. M. Navon, 1988: Variational and optimization methods in meteorology: a review. *Tech. Rep. FSU-SCRI-88-144*, Florida State University, Tallahassee, Florida, 83 pp.

Le Dimet, F. X., and O. Talagrand, 1986: Variational algorithms for analysis and assimilation of meteorological observations: Theoretical aspects. *Tellus*, **38A**, 97-110.

Liu, D. C., and J. Norcedal, 1989: On the limited memory BFGS method for large scale optimization. *Math. Prog.*, **45**, 503-528.

Liu, Z., 1999: Planetary wave modes in thermocline: Non-Doppler-shift mode, advective mode and Green mode. *Q. J. R. Meteorol. Soc.*, **125**, 1315-1339.

Lorenc, A. C., 1981: A global three-dimensional multivariate statistical interpolation scheme. *Mon. Wea. Rev.*, **109**, 701-721.

- Lorenc, A. C., 1988: Optimal nonlinear objective analysis. *Q. J. R. Meteorol. Soc.*, **114**, 205-240.
- Martin, P. J., 2000: A description of the Navy Coastal Ocean Model Version 1.0, *NRL/FR/7322-009962* pp 39., Nav. Res. Lab., Stennis Space Center, Miss.
- Morey, S. L., P. J. Martin, J. J. O'Brien, A. A. Wallcraft, and J. Zavala-Hidalgo, 2003: Export pathways for river discharged fresh water in the northern Gulf of Mexico. *J. Geophys. Res.*, **108**, C10, 3303, doi:10.1029/2002JC001674
- Navon, I. M., and D. M. Legler, 1987: Conjugate gradient methods for large scale minimization in meteorology. *Mon. Wea. Rev.*, **115**, 1479-1502.
- Navon, I. M., X. Zou, J. Derber, and J. Sela, 1992: Variational data assimilation with an adiabatic version of the NMC spectral model. *Mon. Wea. Rev.*, **122**, 1433-1446.
- Panofsky, H., 1949: Objective weather-map analysis. *J. Appl. Meteor.* **6**, 386-392.
- Philander, S. G., 1990: *El Niño, La Niña, and the southern oscillation*, pp. 160-167, Academic Press, Inc., New York.
- Sasaki, Y. K., 1955: A functional study of the numerical prediction based on the variational principle. *J. Meteor. Soc. Japan*, **33**, 262-275.
- Sasaki, Y. K., 1958: An objective analysis based on the variational method. *J. Meteor. Soc. Japan*, **36**, 77-88.
- Sasaki, Y. K., 1969: Proposed inclusion of time-variation terms, observational and theoretical in numerical variational objective analysis. *J. Meteor. Soc. Japan*, **47**, 115-203.
- Sasaki, Y. K., 1970(a): Some basic formalisms in numerical variational analysis. *Mon. Wea. Rev.*, **98**, 857-883.
- Sasaki, Y. K., 1970(b): Numerical variational analysis formulated under the constraints as determined by long-wave equations as a low-pass filter. *Mon. Wea. Rev.*, **98**, 884-898.
- Sasaki, Y. K., 1970(c): Numerical variational analysis with weak constraint and application to the surface analysis of severe storm gust. *Mon. Wea. Rev.*, **98**, 899-910.

- Shriver, J. F., M. A. Johnson, and J. J. O'Brien, 1991: Analysis of remotely forced oceanic Rossby waves off California. *J. Geophys. Res.*, **96**, C1, 749-757.
- Siegel, D. A., D. J. Mcgillicuddy, Jr., E. A. Fields, 1999: Mesoscale eddies, satellite altimetry, and new production in the Sargasso Sea. *J. Geophys. Res.*, **104**, C6, 13359-13379.
- Shu, L., and A. J. Clarke, 2002: Using an ocean model to examine ENSO dynamics. *J. Phys. Oceanogr.*, **32**, 903-923.
- Talagrand, O., and P. Courtier, 1987: Variational assimilation of meteorological observations with the adjoint vorticity equation. Part I: Theory. *Q. J. R. Meteorol. Soc.*, **113**, 1311-1328.
- Thiebaux, H. J. and M. A. Pedder, 1987: Spatial objective analysis. Academic Press, pp 299.
- Yu, L., and J. J. O'Brien, 1991: Variational estimation of the wind stress drag coefficient and the oceanic eddy viscosity profile. *J. Phys. Oceanogr.*, **21**, 709-719.
- Yu, P., S. L. Morey, and J. Zavala-Hidalgo, 2004: New mapping method to observe propagating features. *Sea Technology*, **45(5)**, 20-24
- Zou, X., I. M. Navon, and F. X. Le Dimet, 1992: An optimal nudging data assimilation scheme using parameter estimation. *Q. J. R. Meteorol. Soc.*, **118**, 1163-1186.
- Zou, X., I. M. Navon, M. Berger, K. H. Phua, T. Schlick, and F. X. Le Dimet, 1993: Numerical experience with limited-memory quasi-Newton and truncated Newton methods. *SIAM Jour. On Numerical Optimization.*, **3**, 582-608.
- Zou, X., Y.-H. Kuo, and Y.-R. Guo, 1995: Assimilation of Atmospheric Radio Refractivity using a nonhydrostatic adjoint model. *Mon. Wea. Rev.*, **123**, 2229-2250.
- Zou, X., F. Vandenberghe, M. De Pondeca, and Y.-H. Kuo, 1997: Introduction to adjoint techniques and the mm5 adjoint modeling system. *NCAR Technical Note, NCAR/TN-435-STR*, pp 122.

BIOGRAPHICAL SKETCH

Degrees

M.S. in Physical Oceanography, Ocean University of China
June 1999, Qingdao, China

B.S. in Oceanography, Ocean University of China
June 1996, Qingdao, China

Publications

Yu, P., S. L. Morey, and J. Zavala-Hidalgo, 2004: New mapping method to observe propagating features, *Sea Technology*, 45(5), 20-24

Yu, P., S. L. Morey, and J. J. O'Brien, 2004: Development of a reduced space adjoint data assimilation technique for numerical simulation of oceanic circulation, in *Research Activities in Atmospheric and Ocean Modeling*, Report No. 34, Edited by J. Cote, pp. 08.21-08.22, World Meteorological Organization, Geneva, Switzerland

Yu, P., J. Zavala-Hidalgo, and J. J. O'Brien, 2003: A new mapping method for satellite altimeter data, in *Research Activities in Atmospheric and Ocean Modeling*, Report No.33, Edited by J. Cote, pp. 08.18-08.19, World Meteorological Organization, Geneva, Switzerland

Zavala-Hidalgo, J., P. Yu, S. L. Morey, M. A. Bourassa, and J. J. O'Brien, 2003: A new interpolation method for high frequency forcing fields, in *Research Activities in Atmospheric and Ocean Modeling*, Report No. 33, Edited by J. Cote, pp. 03.21-03.22, World Meteorological Organization, Geneva, Switzerland

Yu, P., J. Zavala-Hidalgo, S. L. Morey, and J. J. O'Brien, 2003: A new mapping method for propagating data, *Oceans 2003 Extended Abstract*

Zavala-Hidalgo, J., M. A. Bourassa, S. L. Morey, J. J. O'Brien, and P. Yu, 2003: A new temporal interpolation method for high-frequency vector wind fields, *Oceans 2003 Extended Abstract*

Yu, P., 1999: Study of the empirical mode decomposition and Hilbert spectrum and its application, *M.S. Thesis*

Zhang, S., P., Yu, 1999: Application of Walsh spectrum onto nonlinear stochastic processes, *Transactions of Oceanology and Limnology*, 1999(2), 1-5

Professional Organizations

American Geophysical Union

Awards

Outstanding graduate student Awards, Ocean University of China, China, 1996—1997

Field Experience

NOAA Ship *Ka'imimoana*, Pacific Ocean, May-June, 2001

OUQD Ship *Dong Fang Hong*, East China Sea Hydrographic Survey, 1997

OUQD Ship *Dong Fang Hong*, East China Sea Hydrographic Survey, 1993